Microscopic Mechanism of Contraction of Tension Wood G-Fiber Due to Boiling

Hiroyuki Yamamoto (hiro@agr.nagoya-u.ac.jp)
Nagoya University
K.C. Sujan
Agriculture and Forestry University
Miyuki Matsuo-Ueda
Kyoto University - Uji Campus: Kyoto Daigaku - Uji Campus
Masato Yoshida
Nagoya University Graduate School of Bioagricultural Science and School of Agricultural Sciences: Nagoya Daigaku Daigakuin Seimei Nogaku Kenkyuka Nogakubu
Shuoye Chen
Kyoto University Graduate School of Agriculture Faculty of Agriculture: Kyoto Daigaku Nogaku Kenkyuka Nogakubu

Research Article

Keywords: hemicellulose, dimensional stability, growthstress, drying shrinkage, gelatinouslayer

Posted Date: March 3rd, 2022

DOI: https://doi.org/10.21203/rs.3.rs-1357896/v1

14th Feb 2022

Microscopic mechanism of contraction of tension wood G-fiber due to boiling

Hiroyuki Yamamoto[1 *], K.C. Sujan[1,2], Miyuki Matsuo-Ueda[1,3], Masato Yoshida[1], Shuoye Chen [1,4]

1 Graduate School of Bioagricultural Sciences, Nagoya University, Chikusa, Nagoya 464-8601, Japan

*: corresponding author hiro@agr.nagoya-u.ac.jp

2 Agriculture and Forestry University, Rampur, Chitwan, Nepal

3 Research Institute for Sustainable Humanosphere, Kyoto University, Uji, Kyoto 611-0011, Japan

4 Graduate School of Agriculture, Kyoto University, Kitashirakawa, Oiwake-cho, Sakyo-ku, Kyoto 606-8502, Japan

Abstract Many woody eudicot plants form a secondary xylem composed of gelatinous fibers (G-fibers) called "tension wood" (TW) along the upper side of the tilted stem or branch. TW generates a large tensile growth stress in the longitudinal direction, allowing the tilted stem or a branch to develop negative-gravitropism in response to the strong gravitational stimulus. This is because the G-fibers tend to contract in the longitudinal direction as they mature. The matured G-fibers also contract upon boiling treatment in water (= hygrothermal treatment). These contractions occur in the gelatinous layer (G-layer) as an innermost layer of the G-fiber. It is still an unsolved mystery how the G-layer, which is composed of highly crystallized and longitudinally oriented cellulose microfibrils (CMFs), contracts during cell wall maturation or during hygrothermal treatment.

In the present study, TW specimens of Konara oak (*Quercus serrata* L) were subjected to hygrothermal treatments under different temperature and time conditions, and strains due to treatment were followed. Besides, the mass loss due to hygrothermal treatment was also followed. From analyzing the obtained results, physical behavior of CMF and other non-cellulosic matrix components in the G-layer during the hygrothermal treatment was estimated. The discussion was further developed to associate hygrothermal contraction with microscopic mechanisms of the contraction of the tension wood G-fiber during maturation.

Keyword: hemicellulose, dimensional stability, growth stress, drying shrinkage, gelatinous layer

Authors' information (name, present affiliation, and e-mail address (ORCID ID)

Hiroyuki YAMAMOTO
Graduate School of Bioagricultural Sciences, Nagoya University, Chikusa, Nagoya 464-8601, Japan
hiro@agr.nagoya-u.ac.jp
ORCID: https://orcid.org/0000-0003-3288-3058

K.C. Sujan
Agriculture and Forestry University, Rampur, Chitwan, Nepal
1rocknroll23@gmail.com

Miyuki Matsuo-Ueda
Research Institute for Sustainable Humanosphere, Kyoto University, Uji, Kyoto 611-0011, Japan
matsuo.miyuki.4d@kyoto-u.ac.jp
OCRID: https://orcid.org/0000-0002-4149-302X

Masato Yoshida
Graduate School of Bioagricultural Sciences, Nagoya University, Chikusa, Nagoya 464-8601, Japan
yoshida@agr.nagoya-u.ac.jp
OCRID: https://orcid.org/0000-0002-5904-0459

Shuoye Chen
Graduate School of Agriculture, Kyoto University, Kitashirakawa, Oiwake-cho, Sakyo-ku, Kyoto 606-8502, Japan
chenshuoye@gmail.com
ORCID: https://orcid.org/0000-0001-6950-1856

List of Abbreviations:

TW: tension wood

NW: normal wood

OW: opposite wood

LW: lateral wood

G-fiber: gelatinous fiber

N-fiber: normal fiber

G-layer: gelatinous layer

L-layer: lignified layer

CMF: cellulose microfibril

MFA: microfibril angle

HTR: hygrothermal recovery

HTR-strain: hygrothermal recovery strain

HT-treatment: hygrothermal treatment

HTR-behavior: hygrothermal recovery behavior

XRD: X-ray diffraction

WAXS: wide angle X-ray scattering

$FWHM_{\beta}$: Full width at half maximum of central peak in β-profile

$FWHM_{200}$: Full width at half maximum of 200 peak in WAXS-profile

O.I. : orientation index of CMF in the secondary wall of wood fiber, equivalent to $FWHM_{\beta}$ in β-profile

C.I. : crystallinity index of CMF in the secondary wall of wood fiber, calculated by Eq.3

WSC : width of single crystallite of cellulose, calculateed by Eq.4

Introduction

Many of woody eudicot species often form the tension wood (TW) with the gelatinous fiber (G-fiber) along the upper side in their tilted stems or branches, where a large tensile growth stress is generated in the longitudinal direction. This is because each G-fiber tends to contract in its longitudinal direction during the maturation of the cell wall (*e.g.*, Okuyama et al. 1990: ibid. 1994; Yamamoto et al. 2005; Clair et al. 2003; Gril et al. 2017). This helps the hardwood stem and branch to maintain their species-specific shapes against the gravitational stimulus during its secondary growth (*e.g.*, Yamamoto et al. 2002; Fourcaud et al. 2003; Gril et al. 2017). On the other hand, the formation of TW often causes obstacles when we human beings process harvested logs into the structural lumbers. When a log containing the TW is sawn, resulting primary lumbers are irregularly warped, and/or cracked because the residual stress balanced in the log is redistributed by sawing (*e.g.*, Kübler and Chen 1974; Okuyama et al. 2004; Kang et al. 2007).

In addition, TW contracts further in the longitudinal direction due to moisture release, which results in even greater warping and cracking of the primary lumbers after drying. In severe cases, this can lead to serious failures such as longitudinal cleavage and end splitting. Defects due to drying are particularly serious when subjected to industrial kiln-drying treatment (high temperature drying) (*e.g.*, Kang et a. 2007; Tarmian at al. 2009; Vilkovska et al. 2019). Some researchers believe that at the early stages of the high-temperature drying process, contraction of fiber called "hygrothermal recovery (HTR)" occurs along the longitudinal direction, which is unusually high especially for the G-fiber (Abe and Yamamoto 2007, Clair 2012, Sujan et al. 2015, ibid 2016, Chen et al. 2021; Vilkovska et al. 2019). After the drying treatment, it is necessary to give correction sawing to the dried lumber and remove damaged and/or warped parts in it, resulting in an extreme decrease of utilization yield of the harvested logs.

Many researchers consider that behaviors peculiar to the TW are attributable to the contractile nature of cellulose-rich G-layer (Okuyama et al. 1990; ibid 2004; Clair and Thibaut 2001; Clair et al. 2003; ibid 2008; Yamamoto et al. 1992; ibid 1993a; ibid 2005; ibid 2010; Chen et al. 2021); in other words, the G-layer tends to contract in the longitudinal direction during cell wall maturation, contract again by hygrothermal treatment (HT-treatment), and contract further by moisture desorption. The strains caused by these three types of contraction are called "maturation strain," " hygrothermal recovery strain," and "drying shrinkage strain," respectively. Recently, some researchers have mentioned the role of matrix polysaccharide entrapped in the cellulose microfibrils (CMFs) of the G-layer in generating the abnormal tensile growth stress in the TW. Early authors considered that xyloglucans (XG) and xyloglucan endo-transglucosylase (XET) take part in inducing tensile stress in G-layer (e.g., Nishikubo et al. 2007; Mellerowicz et al. 2008; Baba et al. 2009); however, recent studies clarified that the main matrix substance are globular polysaccharides of rhamnogalacturonan I (RG-1), arabinogalactan protein (AGP), and acidic galactan, which are sandwiched between CMFs of the G-layer (Bowling et al. 2008; Sandquist et al. 2010; Mellerowicz et al. 2012; Gorshkova et al. 2015; Almeras and Clair 2016; Guede et al. 2017). They propose a theory that volume growth of the globules causes a lateral expansion, resulting an axial contraction of the G-layer.

On the other hand, the mechanisms of other two longitudinal contractions of the G-layer, which causes hygrothermal recovery strain (HTR-strain) and drying shrinkage strain in the G-fiber, are not yet sufficiently discussed compared to the case of maturation strain without some exceptions (Abe and Yamamoto 2007; Clair 2012; Sujan et al. 2015; ibid 2016; Capron et al. 2018). It is natural to consider that these three kinds of contraction would interrelate each other at the level of the fine composite structure of the G-layer. Clarifying the commonalities and differences among these three contractile behaviors would ultimately lead to understanding the mechanism of each contraction of the G-layer.

Kübler (1959), Yokota and Tarkow (1962), Sasaki and Okuyama (1983), Gril et al. (1993), and Gril and Thibaut (1994) were pioneer researchers involved in systematically investigating the hygrothermal recovery behaviors (HTR-behaviors) of wood. They revealed that the normal wood (NW) specimen expands by 0.5 % to 1% in the tangential direction due to the HT-treatment, while it contracts by about half of that in the radial direction. There is virtually no dimensional change in the longitudinal direction. Later, researchers reported that the reaction wood specimen changes its dimension significantly in the longitudinal direction. Softwood compression wood expands by 0.5-1.0 % (Tanaka et al. 2014; Matsuo et al 2016), while hardwood TW made of G-fibers contracts by up to 2-3 % due to the HT-treatment (Abe and Yamamoto 2007; Clair 2012; Sujan et al. 2015, 2016, 2018; Capron et al. 2018). Some of these authors consider that some amount of the growth stress remains in the cell wall even after the elastic component was released by separating the wood specimen from the living stem, which is then viscoelastically released by hygrothermal softening (HT-softening), causing HTR-strain. This explains the macroscopic HTR-behavior of wood, not the microscopic mechanism of HTR-strain and its relationship to the other two types of contraction in TW, based on quantitative data and convincing theory. How the G-layer, which consists of rigidly crystallized and longitudinally oriented CMFs, contracts during cell wall formation and during HT-treatment remains an unsolved mystery.

In the present study, based on the above background, wood specimens containing various amount of G-fiber were collected from the tilted stem of Konara oak (*Quercus serrata* L), and they were subjected to HT-treatments under different temperature and time conditions, and the strains of HTR were compared among the various treatment conditions. From analyzing the obtained results, HTR-behaviors of CMF and other non-cellulosic matrix components in the G-layer were estimated. Moreover, the discussion would extend to associate HTR-behaviors with microscopic mechanisms of the other two characteristic contractions in the G-fiber, *i.e.*, maturation strain and drying shrinkage: this will include a critical discussion of the aforementioned theory that globule-like matrix polysaccharides are involved in the generation of G-fiber maturation strain.

Material and Method

Material tree and specimen preparation

Tested species and sampling site

At the Experimental Forest of Nagoya University (Inabu mountainous district, Toyota City, Aichi Prefecture, Japan), a 19-year-old Konara oak (*Quercus serrata* Thunb.) (breast-height diameter 12.5 cm) that had grown on a steep slope was used as the tested tree. The inclination of the stem axis at breast height was approximately 11-13° with respect to the vertical axis. At a height of 120 cm above the ground (hereinafter, called as "Height 120"), three specimen-sampling points were circumferentially marked on the upper side of the tilted stem (*i.e.*, concave side, where formation of the G-fiber is expected to develop) and one on the opposite side (*i.e.*, convex side): at a height of 165 cm above the ground (hereinafter, called as "Height 165"), three, two, one specimen-sampling points were circumferentially marked on the upper, lateral, and opposite sides of the tilted stem, respectively (see **Fig. 1**).

Fig. 1 Schematic representation of tested tree and specimen preparation

Prior to specimen sampling, longitudinal release strains of surface growth stress were measured at five marked points on the upper and lateral sides of "Height 165" to evaluate the degree of G-fiber formation in the tested tree (see **Fig. 1**). The strain-gauge method was adopted to measure the released strain in a tilted stem (Okuyama et al. 1981; Yamamoto et al. 1989; Yoshida and Okuyama 2002). In the TW containing a large amount of the G-fiber, it is expected to detect a negative value of the longitudinal released strain with an absolute value of more than 0.15 %; while, in the NW without forming G-fiber, the absolute value is 0.05% or less (Okuyama et al. 1990; ibid.1994; Yamamoto et al.1992). If neither is the case, the degree of development of the G-fiber formation would remain moderate or low. In this way, it is possible to efficiently collect samples with different degrees of development of G-fibers in addition to N-fibers by referring to the measurement results of longitudinal released strain of surface growth stress.

Specimen preparation

After that, a log with a length of 12 cm was cut from directly above "height 120" (call it as "log A", hereinafter), and also directly below "Height 165" (call it as "log B", hereinafter), and immediately transferred to the Laboratory of Wood Physics, Nagoya University (Chikusa, Nagoya, Japan) in a sealed plastic bag. From each peripheral position corresponding to the marked point, one piece (log B) or two pieces (log A) of long rectangular portion with a length (longitudinal) of 110~120 [mm], a width (tangential) of 20mm and thickness (radial) of 7~8 [mm] were cut, and each portion was divided into 5~7 rectangular specimen of which dimension was length of 15 [mm], width of 15 [mm], and thickness of 5 [mm]. Healthy specimens without defects, such as knot and/or curved grain, were selected. After preparation, all specimens were stored in a fresh running water tank at room temperature so as not to

dry. Those operations were done in November 2017.

Measurement of dimensions of specimen

After keeping each specimen in a running water tank at room temperature 25±2 [℃] for one week, the green dimensions of the specimen (longitudinal length $l_L(0)$ [mm] and the tangential length $l_T(0)$ [mm]), sampled from logA, were measured at room temperature. Immediately after immersing the specimen in a water tank with a treatment temperature of θ [℃] for a certain duration t [min], the specimen was rapidly cooled with ice and water in a 200 [ml] small beaker, and left unattended (12 [hour] or more) until the water temperature became equilibrated to room temperature. Then, at room temperature, the longitudinal length $l_L(t)$ [mm] and the tangential length $l_T(t)$ [mm] were measured at cumulative duration t [min] since starting the first HT-treatment.

Dimensions $l_L(t)$ and $l_T(t)$ were recorded with a reading accuracy of 0.001 [mm] based on the method described in Tanaka *et al.* (2014). The HTR-strains $\varepsilon_L(t)$ and $\varepsilon_T(t)$ of the specimen having a cumulative treatment duration t [min] were calculated by the following equation (Tanaka et al. 2014).

$$\varepsilon_L(t) = \frac{\left(l_L(t) - l_L(0)\right)}{l_L(0)} \times 100 \quad (\%), \qquad \varepsilon_T(t) = \frac{\left(l_T(t) - l_T(0)\right)}{l_T(0)} \times 100 \quad (\%) \tag{1}$$

HT-treatment

Experiment 1- dimensional change due to HT-treatment

Treatment of Phase 1: Total 40 specimens cut from log A were evenly divided into 5 equivalent groups (G1, G2, G3, G4, G5), and were used for Experiment 1. Those were subjected to the HT-treatment temperatures at 40, 60, 80, 100, 120 [℃], respectively. For treatment groups G1, G2, G3, and G4, a HT-treatment was performed by immersing the specimen in a heated water tank under normal room pressure. For treatment group G5, HT-treatment was performed using a sterilization autoclave (Pasolina, IST-150, Japan).

A short time treatment (30 or 60 [min]) was given to the groups G2, G3, G4, and G5 as the initial HT- treatment, followed by repeated treatments of 60 to 150 [min] (maximum 240 [min]). For group G1, long time treatments of 1000 to 2000 [min] were repeatedly performed from the initial stage of the treatment since the HT-treatment does not cause so rapid HTR-strain at a comparatively low temperature (40 [℃]).

Treatment of Phase 2: For groups G1, G2, G3, and G4, the HT-treatment temperature was increased by 10 to 15 [℃] when the longitudinal HTR-strain of the specimen became almost constant due to the progress of the HT-treatment in Phase 1. Then, the HT-treatment of Phase 2 was continued. Specimens group G5 (treated at 120 [℃]) were not treated at higher temperatures.

Treatment of Phase 3:

For groups G1, G2, G3 and G4, all specimens were subjected to the HT-treatment at 120 [℃] when the longitudinal HTR-strain became almost constant due to the progress of the HT-treatment in Phase 2. Then, the HT-treatment of Phase 3 was continued. When the measured value of the longitudinal HTR-strain reached almost constant in Phase 3, the HT-treatment was ceased.

The obtained results in Experiment 1 were used for discussing the relationships between the longitudinal and tangential HTR-strains and the cumulative treatment duration.

Experiment 2 – degradation due to HT-treatment

As the HT-treatment proceeds, the specimen possibly undergoes degradation (*e.g.*, Tejada et al. 1998; Garrote et al. 2001; Kim et al. 2001). By soaking the wood in hot or cold water, some extractive components in the cell wall and lumen are removed. As the HT-treatment proceeds, some cell wall components become low molecular weight due to degradation, which are also extracted and removed (*e.g.*, Fengel 1984). As a result, mass decrease is thought to occur in the HT-treated specimen. Thermal degradation could affect the dimensions of the specimen in the longitudinal and the tangential directions, which in turn would affect the HTR-strain.

Total 18 specimen cut from log B were evenly divided into three treatment groups G6, G7, and G8 (see **Fig. 1**), which were used to track the change in mass of specimen with the progress of the HT-treatment. First, the green specimens were air-dried in a room environment. The specimens were then placed in a drying oven set at 60 [℃] for 24-36 [h] and then dried at 105 [℃] for 6-7 [h]. The specimen was then left to cool in a desiccator with silica-gel for 15 [min] at room temperature, and the mass M (0) [g] was weighed and regarded as the oven-dry mass of the untreated specimen. After that, the dried samples were again immersed in water under room temperature to achieve water saturation, and the HT-treatment was then performed according to a predetermined temperature and time schedule. The same procedure was used to measure the oven-dry mass $M(t)$ [g] of the specimen, where t is cumulative treatment duration since the initial heating in Experiment 2.

In Experiment 2, the following equation was used to calculate the ratio of mass change $\delta(t)$ [%] when HT-treatment was performed with a cumulative treatment time t [min] from initial heating.

$$\delta(t) = \frac{\big(M(t) - M(0)\big)}{M(0)} \times 100 \quad (\%) \tag{2}$$

The value of $\delta(t)$ is negative, and its absolute value indicates the degree of degradation of the specimen due to HT-treatment. In Experiment 2, three kinds of treatment schedule were set using three temperatures conditions, 80, 100, and 120 [℃] (see also **Fig. 10**).

Quantitative evaluation of degree of development of TW by X-ray diffraction (XRD) measurement

The G-layer consists of a high concentration of cellulose microfibril (CMF) of which longitudinal axis is more or less oriented along the longitudinal axis of the G-fiber (Onaka 1949; Wardrop and Dadswell 1955; Côté and Day 1962; Araki et al. 1982; Okuyama et al. 1994). Those structural properties are clearly reflected in the X-ray

diffraction (XRD) patterns of the specimen (Wardop and Dadswell 1955; Wada et al. 1995; Muller et al. 2006; Yamamoto et al. 2010 ; Leppanen et al. 2011; Sujan et al. 2015). This indicates that degree of TW development could be evaluated by the XRD measurement. Then, in the present study, after the completion of series of measurements in Experiment 1, degree of the development of G-fibers in each specimen was analyzed by the XRD measurement.

Using a utility knife, each specimen was divided into two tangential sections of which thickness was 2-3 mm, tangential length was 13-14 mm, and longitudinal length was 14 -15 mm. After the sections were air-dried at room temperature, the samples were subjected to XRD measurements on an X-ray diffractometer (Ultima IV, Rigaku, Tokyo, Japan) using CuKα (λ = 0.15406 nm) generated at 40 kV × 40 mA. Scattered X-ray was detected by the scintillation counter after monochromatization with graphite 0002. In the wide-angle X-ray-scattering (WAXS) measurement, a wood section was placed in the center of the goniometer so that the fiber axis of the section coincided with the rotation axis of the goniometer, and diffraction profile was recorded from 2θ = 5° to 40° in a symmetrical reflection mode (*i.e.*, Bragg and Brentano geometry) with a step size of 0.01° at a scanning rate of 3 [°/min]. From the WAXS-profile, the degree of crystallinity of the cell wall substance (crystallinity index; *C.I.*) and the width of single crystallite of cellulose (*WSC*) were estimated (see eqs.(3) and (4), and **Fig. 2**).

In the β-profile measurements, a fiber-specimen attachment (Rigaku, Tokyo, Japan) was set in the goniometer so that its rotation axis made an angle of 11.2 ~ 11.3° with the incident X-ray beam. The tangential section of wood was irradiated with the incident X-ray in a symmetric transmission mode, and the diffraction intensities along 200 arc of cellulose I_β were recorded from $\beta = -75°$ to +90° with a step size of 0.5°. From the β-profile, the degree of orientation of CMF in the cell wall (Orientation index; *O.I.*) was measured (see **Fig. 3**).

Fig. 2 Typical WAXS profiles of solid wood sections of (a) TW and (b) NW. From WAXS profile, values of *C.I.* (crystallinity index) and *WSC* (width of single crystallites) of CMF are calculated using Eqs.(3) and (4), respectively. Linear background was already eliminated in each profile.

Fig. 3 Typical β-profiles of solid wood sections of (a) TW and (b) NW specimen. From β-profile, an *O.I.*, (= full width of half maximum in the diffraction peak ($FWHM_\beta$)) is calculated. Value of *O.I.* is a convenient indicator of the average MFA in the cell wall. Linear background was already eliminated in each profile.

In advance that those parameters were calculated from XRD profiles, each profile must be peak-fitted and smoothed after eliminating the linear background. WAXS profile was smoothed by the simple superposition of several Lorentzian functions corresponding to typical diffraction peaks of cellulose I_β crystal and the amorphous hallo as shown in **Fig. 2**. The β-profile was also smoothed by the simple superposition of Lorentzian functions corresponding to diffraction arcs from the secondary wall and G-layer (see, **Fig. 3**). When fitting both profiles, the least square method using Excel solver (Microsoft 365) was adopted.

C.I. was defined by the following formula with reference to Segal (1959), Toba et al. (2013), Agarwal et al.

(2017), and so forth:

$$C.I.[\%] = \frac{I_{200} - I_{amor}}{I_{200}} \times 100 \quad (3),$$

where I_{200} and I_{amor} are respectively the maximum intensity at 200 peak and the minimal intensity around 2θ =18° in the WAXS profile which was smoothed after eliminating the background.

The value of *WSC* was calculated from the following Scherrer's formula (*e.g.*, Agarwal et al. 2017), assuming that instrumental broadening could be negligible in the present measurement:

$$WSC\ [nm] = \frac{K \cdot \lambda}{B \cdot \cos\theta_{200}} \quad (4),$$

where K is Scherrer's constant (= 0.9): λ is a wavelength of CuK_α radiation (= 0.15406 [nm]): B is a full width at half maximum ($FWHM_{200}$) in the deconvoluted 200 diffraction peak: θ_{200} is Bragg's angle of the 200 diffraction.

The value of *O.I.* was evaluated by the full width at the half maximum ($FWHM_\beta$) of the main peak in the β-profile, which was smoothed after removing the background. The Cave's *angle T* is also well known as a convenient indicator of so-called average microfibril angle (MFA) of softwood and normal hardwood specimens (*e.g.*, Meylan 1967; Cave 1966; Yamamoto et al. 1993b; Tanaka et al. 2014): this is basically proportional to the $FWHM_\beta$ of the main peak in the β-profile, *i.e.*, *O.I.*. Sujan et al (2015) applied the idea of *angle T* to the specimens of Konara-oak (*Q. serrata*) and Urihadakaede-maple (*A. rufinerve*) containing G-fiber, and they revealed that the *angle T* decreases as the proportion of G-fibers increases. This can be explained by the fact that the CMF of the G-layer are oriented along the fiber axis in the G-fiber, and that the *angle T* or $FWHM_\beta$ are convenient indicators of the degree of development (composition ratio) of G-fiber. Hence, in the present study, *O.I.* was adopted as a simpler and more convenient indicator of TW development in each specimen.

Results and discussion

Detection of TW formation by the released strain of the growth stress in a standing tree

Contractile released strains of −0.18 ~ −0.25 % were detected on the upper side of the tilted stem of the tested tree (at the measurement point 2, 3, and 4 of "Height 165" in **Fig. 1**), while values of −0.046 and −0.094% were detected on the lateral sides (at 1 and 5 at "Height 165"). In the present study, released strain was not measured on the opposite side; however, it has been empirically known that on the opposite side in a tilted stem, the longitudinal released strain is normally a small contractile value of which absolute value varies in the range of 0 ~ 0.05 % and that no G-fiber is formed (*e.g.*, Okuyama et al. 1990; ibid. 1994).

Considering all these results, it was concluded that the tested tree was likely to form a developed TW on the upper side of the tilted stem, while the NW was formed on the opposite and part of lateral sides.

Evaluation of degree of TW development by the XRD measurement

The specimen sampled from the upper side of the tilted stem often showed WAXS-profiles typical of pure crystallized cellulose I (see **Fig. 2a**), which was identified as TW specimen. In contrast, specimens prepared from lower (=opposite) side showed profiles typical of cellulose I in lignified cell walls (see **Fig. 2b**), which was identified as NW specimen. In the former cases, the $1\bar{1}0$ and 110 peaks at 2θ = 15~17° were more or less separated, but in the latter cases, these peaks were not separated but were rather a single broad peak. The width of the 200 peak at 2θ = 22.2~22.6° was smaller in the TW specimens (**Fig. 2a**) than in the NW specimens (**Fig. 2b**), and the ratio of the intensity of the 200 peak to that of the amorphous halo at 2θ = 18° was larger in the TW specimens than in the NW specimens. There was no visible indication for the degradation and/or phase transformation of cellulose crystal structure. Those characteristics coincided with the previously reported results (e.g., Wardop and Dadswell 1955; Wada et al. 1995; Muller et al. 2006; Leppanen et al. 2011; Yamamoto et al. 2010).

The β-profiles of both the TW and the NW specimens showed single peaks symmetrical with respect to the rotation (azimuthal) angle β, but *O.I.* of the former was much smaller and the diffraction intensity at the symmetry axis was larger than the latter (see **Fig. 3a,b**). Some specimens sampled from the upper side of the tilted stem fell into intermediate categories between the developed TW and the NW both for WAXS and β-profiles. In such specimens, G-fibers are formed, but their ratio is not considered to be very high.

The above results indicate that the developed TW specimen contains much amount of G-layer, which consists of a large amount of highly crystallized CMF that are oriented in the direction parallel to the longitudinal axis of the G-fiber. On the other hand, in NW specimen, CMF is oriented more or less inclined to the longitudinal axis of the fiber, which may result in a broader β-profile; furthermore, crystallization of the cell wall is relatively prevented by the deposition of lignified matrix substance. Based on the method described above, all specimens used were classified as either tension wood or normal wood.

Experiment 1

HTR-strain in the longitudinal direction

In the treatment of Phase 1, specimen containing G-fiber (*i.e.*, TW specimen) showed irreversible contraction (= negative HTR-strain) in the longitudinal direction. In the treatment groups G1, G2, and G3, the TW specimen shrank exponentially as the treatment progressed, and eventually converged to each fixed value. In the treatment groups G4 and G5, a rapid contraction, called "*initial recovery*" by Sujan et al. (2015), was remarkably observed at the beginning of the treatment, and then the contraction continued slowly, which was called "*continuum contraction*" by Sujan et al. (2015). It eventually converged to each fixed value **(Fig. 4**). Those coincided with the previous results reported by Sujan et al. (2015, 2016). The NW specimen showed almost no dimensional change. However, in the treatment group G5, the specimen shrank linearly with the progress of treatment as shown in **Fig. 4**. The magnitude of the contraction in NW specimen, however, was not nearly as large as that shown by the TW specimen.

Fig. 4 Time-dependent evolutions of longitudinal HTR-strains in Experiment 1

In the treatment of Phase 2, the HT-treatment temperature was increased by 10 [℃] in G1, G2, and G3, and by 15 [℃] in G4. The TW specimen further shrank exponentially regardless of treatment temperatures, and eventually converged to each fixed value. The NW specimen showed almost no dimensional change except group G4 where specimen shrank linearly with the progress of treatment (see **Fig. 4**).

In the treatment of Phase 3, all specimens were subjected to the HT-treatment at 120 [℃]. The TW specimen shrank rapidly but exponentially regardless of treatment groups. The NW specimen also shrank linearly regardless of treatment groups as shown in **Fig. 4**. However, the magnitude of the contraction in NW specimen was not nearly as large as that shown by the TW specimen regardless of treatment groups.

Figures 5(a) and **5(b)** show the relationships between the longitudinal HTR-strains and the treatment temperatures at the end of Phase 1 and Phase 2, respectively. For both phases, the specimens that showed the larger HTR-strains in each group were all TW specimens. In both Phase 1 and Phase 2, the higher the treatment temperature group, the greater the longitudinal HTR-strain in developed TW specimens. In addition, the longitudinal HTR-strain at the end of Phase 3 is shown in **Fig. 5(c)**. From **Fig. 5(c)**, it appears that the absolute value of the HTR-strain would increases slightly in the order of G1, G2, ..., G5. However, the one-way ANOVA showed no effect of grouping on the variation of the HTR-strains, which indicates that there is no significant bias in dividing the specimens into five groups, from G1 to G5.

Fig. 5 Longitudinal HTR-strains in each group at the end of Phase 1 (left), Phase 2 (center), and Phase 3 (right)

Fig. 6 Correlations of *O.I.* (orientation index, quantified from $FWHM_\beta$ in β-profile), *C.I.* (crystallinity index, calculated by Eq.3), and *WSC* (width of single crystallite of cellulose, calculated by Eq.4) with the longitudinal HTR-strains at the end of Phase 3 in Experiment 1

Figures 6(a), **(b)**, and **(c)** show correlations of *O.I.* (orientation index, equivalent to $FWHM_\beta$ in β-profile), *C.I.* (crystallinity index, calculated by Eq.3), and *WSC* (width of single crystallite of cellulose, calculated by Eq.4) with longitudinal HTR-strains at the end of Phase 3. These parameters can be considered as indicators of the degree of "TW development" in the anatomical sense. The results of **Fig. 6** shows that the absolute value of longitudinal HTR-strain increases monotonically with the degree of "TW development". This indicates that the specimens with the large absolute values of longitudinal HTR-strains in each group are those with the highly developed TW.

Figure 7 is a composite of **Fig. 5(a)** and **Fig. 5(b)**. It is found that there is a linear relationship between the treatment temperature θ [℃] and the maximum absolute value of the longitudinal HTR strain a_L (solid circle) when the treatment temperature condition is less than 100 °C. The relation was approximated as the following regression line:

$$a_L(\theta)\ [\%] = -0.0339\theta + 1.1387 \quad (R^2 = 0.9947) \tag{5}$$

However, in the regression including treatment groups G4 and G5, a nonlinearity occurred, where the higher the treatment temperature, the greater the contraction.

According to the regression line (Eq. 5), when the HT-treatment temperature is below 33.6℃, the longitudinal

HTR-strain becomes positive, but this cannot happen in practice. Probably, threshold temperature, *i.e*., the lower limit of the treatment temperature at which the TW generates the longitudinal HTR-strain is 33.6 [℃]. As pointed out by Yokota and Tarkov (1961), this may be due to the estimated history that the maximum temperature just beneath the bark of a living tree stem was about 33.6 [℃] in the recent summer season. As a matter of fact, the tested tree was collected from a sunny slope in a mountainous area in Aichi Prefecture, Japan.

Fig. 7 A composite of Fig. 5a and Fig. 5b. A linear relationship was detected between treatment temperature and the maximum absolute value of longitudinal HTR-strain (solid circle) at the end of Phase 1 and Phase 2 for treatment temperatures below 100 [℃].

Fig. 8 Time-dependent evolution of longitudinal HTR-strains for TW and NW in Experiment 1. The curves with the largest (highly developed TW) and smallest (NW) absolute values were picked up from each group in Fig. 4, and they were reconstructed as Fig. 8. Values in the figures are treatment temperatures.

From each group in **Fig. 4**, the curves with the largest (highly developed TW) and smallest (NW) absolute values were picked up, and they were reconstructed in a single figure as **Fig. 8**. It can be clearly understood that the magnitude of the longitudinal HTR-strain in the developed TW is controlled by the treatment temperature, whereas in the NW it does not occur explicitly until the temperature is above 115°C.

Sujan et al. (2015) is the first report referring the characteristic behaviors of the longitudinal HTR-strains in TW specimen, *i.e.*, *initial recovery* and *continuum contraction*. Origins of those behaviors will be discussed in Chapter of General Discussion.

HTR-strain in tangential direction

Figure 9 shows the time-dependent evolution of the tangential HTR-strain in Experiment 1. The curves shown in **Fig. 9** are for the specimens used in **Fig. 8**.

Fig. 9 Time-dependent evolutions of tangential HTR-strains at each treatment group. Displayed curves are for specimens used in Fig. 8.

In the treatment of Phase 1, rapid expansions were observed in the initial stage of treatment except for the group G1 with the treatment temperature of 40[℃]. Thereafter, for treatment groups G1, G2, G3, and G4, the expansion progressed slowly as the treatment progressed and finally converged to their respective constant values. However, in the group G5 with the treatment temperature of 120[℃], the tangential HTR-strain expanded greatly at the very beginning of the treatment and then decreased gradually with the progress of the treatment. A negative value of the tangential HTR-strain was observed in the NW specimen in G5 at the end of Experiment 1.

In the treatment of Phase 2, the HT-treatment temperature was increased by 10 [℃] in G1, G2, and G3, and by

15 [°C] in G4. In treatment groups G1, G2, and G3, the tangential HTR strain increased slightly as the treatment progressed, and soon became constant. In treatment group G4, the tangential HTR-strain once reached the maximum value at the very early stage in Phase 2, and then the dimension decreased slowly as the treatment progressed.

In the treatment of Phase 3, all specimens were subjected to HT treatment at 120 [°C]. For both TW and NW specimens, the tangential HTR-strain increased rapidly at the early stage in Phase 3, but then decreased gradually as the treatment progressed.

Regardless of treatment groups, tangential HTR-strain was found to be greater for the TW specimen than for the NW specimen, as was the case for the longitudinal HTR-strain. However, the quantitative difference in tangential HTR-strain between TW and NW specimen was not as large as in the case of longitudinal HTR strain.

It was revealed that both NW and TW expanded in the tangential direction when HT-treatment was performed at temperatures below 100[°C], and that the tangential HTR-strain became more positive with higher HT-treatment temperatures, even though the correlation was not as high as the longitudinal HTR-strain. When treated at higher temperatures such as 115 [°C] or 120 [°C], the NW and TW expanded rapidly in the tangential direction once at the beginning of the treatment and then turned to contract. Those results suggest that there is an intrinsic difference in the HTR behavior between treatment temperatures below 100[°C] and above 115[°C], which may be attributed to the different modes of thermal degradation at lower and higher treatment temperatures.

The above results do not clearly state whether the HTR-strain in the TW specimens occurred during the HT-treatment or by cooling after the HT-treatment. Matsuo-Ueda et al. (2018) observed the time-dependent evolution of longitudinal HTR-strain of *Zelkova serrata* TW in real time using commercially available strain-gages (KFGS-5-120-C1-11, Kyowa Electronic Instruments, Tokyo, Japan) glued with cyanoacrylate adhesive (CC-33A, Kyowa Electronic Instruments, Tokyo, Japan). The results showed that strain occurred during HT-treatment. Real-time measurement of HTR-strain was also confirmed by early authors (Yokota and Tarkow 1962; Sasaki and Okuyama 1983) on NW specimens of softwood in the longitudinal, the tangential, and the radial directions using an electric displacement-meter. Based on these reports, it is rather natural to consider that the HTR-strains obtained in the present study occurred in the TW during the HT-treatment, both in the longitudinal and tangential directions.

Experiment 2

Treatment of Phase I

In the treatment of Phase I, the treatment groups G6, G7, and G8 were HT-treated under the temperature conditions of 80, 100, and 120 [°C], respectively (see **Fig. 10**). In this treatment phase, all specimens showed a rapid mass loss [%] immediately after the treatment started regardless of groups, and regardless of difference in TW, OW, or LW. In treatment groups G6 and G7, even though the treatment temperature was not changed, there was a sudden braking of the rapid progress of mass loss, followed by a weak mass loss until the end of treatment of Phase I. In contrast to G6 and G7, in treatment group G8, the rapid mass loss continued until the end of Phase I, although there appeared to be a very slight braking at the very beginning of Phase I.

493
494 *Treatment of Phase II*
495
496 In this treatment phase, all the treatment groups were subjected to the HT-treatment with step-functionally
497 reciprocating temperature-schedule between 80 [℃] and 100 [℃], that is, 80 [℃] → 100 [℃] →80 [℃] →100
498 [℃]→80 [℃]. In G6 and G7, a slight mass loss continued until the end of Phase II. In G8, as soon as it entered
499 Phase II, the rapid mass loss that had proceeded in treatment of Phase I stopped abruptly, and thereafter the mass
500 loss proceeded slowly as in G6 and G7. It is considered that the difference of treatment temperature between 80
501 [℃] and 100 [℃] had little effect on the time-dependent pattern of mass loss. In the treatments of Phase I and
502 Phase II, mass loss was greater in TW than in NW (*i.e.*, OW and a part of LW) regardless of treatment groups.
503
504 *Treatment of Phase III*
505
506 In this phase, all the specimens were subjected to the HT-treatment at 120 [℃] for the entire period. All specimens
507 showed a rapid mass loss regardless of treatment group and regardless of difference of TW, OW, or LW. The rapid
508 mass loss continued until the treatment temperature was lowered to 80 [℃] in the subsequent treatment phase.
509
510 *Treatment of Phase IV*
511
512 All groups were subjected to the HT-treatment at 80 [℃]. In this treatment phase, almost no mass loss proceeded
513 regardless of difference of TW, OW, or LW. In the treatment of Phase IV, mass loss was greater in OW than in TW
514 and LW regardless of treatment groups.
515
516 *Treatment of Phase V*
517
518 All groups were subjected to the HT-treatment at 120 [℃]. In all groups, mass loss proceeded rapidly regardless of
519 difference of TW, OW, or LW as in treatment of Phase III. In this treatment phase, mass loss was the largest in the
520 OW specimen regardless of treatment groups.
521
522 **Fig. 10** Mass change rate due to various HT-treatment schedules. Lateral wood specimen often
523 contained G-fiber. Roman numbers on the top of figures stand for HT-treatment phases in Experiment 2.
524
525 *A possible mechanism of HT-degradation of cell wall*
526
527 Regardless of the treatment temperature, a rapid mass loss was observed in Phase I at the very beginning of the
528 treatment, which was probably due to the elution of the extractive components in the fiber lumen or relatively large

529 cavities in the cell wall. After that, the mass loss proceeded very slowly when treated at temperatures below 100
530 [°C] (treatments of Phase II and IV) and there was no substantial difference in the progress of mass loss between 80
531 [°C] and 100 [°C]. On the other hand, the rapid mass loss progressed without stopping when treated at 120 [°C]
532 (treatments of Phase III and V). In the case of treatment below 100 [°C], remaining extractive components and low-
533 molecular-weight components were gradually removed, while in the case of treatment at 120 [°C], some cell wall
534 components were actively decomposed and removed, resulting in rapid mass loss.
535 Many researchers believe that CMF, a crystalline polysaccharide, is rather thermally stable below 300 [°C] (*e.g.*,
536 Kim et al. 2001). This suggests that more non-crystalline matrix components are degraded and removed from the
537 cell wall by 120 [°C] treatment. This could be closely related to the linear increase in the negative value of the
538 longitudinal HTR strain in the NW (see **Fig. 8**), and the rapid decrease in the tangential HTR strain in the TW and
539 the NW specimen (see **Fig. 9**) when treated at 120 [°C]. The time-dependent evolution of longitudinal HTR-strain
540 in TW cannot be explained by the degradation and removal of cell wall matrix components. The mechanism will be
541 discussed in detail in the following Chapter.
542
543 ## General discussion
544
545 ### Why does the G-fiber contract by the HT-treatment? A possible mechanism
546
547 From Experiment 2, it was suggested that the difference of temperature between 80 [°C] and100 [°C] had little
548 effect on the time-dependent evolution of mass loss (see treatments of Phase II and IV in **Fig. 10**). On the other
549 hand, in Experiment 1, it was shown that there was a clear quantitative difference in both longitudinal and
550 tangential HTR-strains between 80 [°C] and 100 [°C] (see **Figs. 8** and **9**). These suggest that there may be some
551 other factor controlling the magnitude of HTR-strain other than the elution of extractives and/or the decomposition
552 of matrix components in the region of treatment temperature less than 100 [°C]. Some early authors reported that
553 even at relatively low temperatures below 100 [°C], the HT-treatment often softens the matrix components of
554 softwood and hardwood cell wall (Goring 1965; Tejada et al. 1998). If we consider that HTR-behavior is caused by
555 delayed recovery of the viscoelastically-locked growth stresses in the cell wall as pointed out by another early
556 authors (Kübler 1959, Yokota and Tarkov 1962; Sasaki and Okuyama 1983; Gril et al. 1993; Gril and Thibaut 1994),
557 then HT-softening may be one of factors accelerating delayed recovery; moreover, the degree of HT-softening of
558 the cell wall may be temperature dependent. In the following, we would like to develop this idea into a more in-
559 depth microscopic mechanism of HTR-behavior in TW based on the results revealed in the present study.
560 Isolating a small wood specimen from a living stem would elastically release some part of the tensile stress
561 generated in the crystalline cellulose microfibril (= CMF) of the G-layer; as the result, the G-fiber contracts
562 instantaneously in its longitudinal direction. In the present study, values of about −0.18~ −0.25 [%] were detected
563 as longitudinal released strains of the surface growth stress (= maturation strain) in a tilted stem of Konara oak. On
564 the other hand, there should still be tensile stress in the CMFs of the G-layer that was not released instantaneously.
565 This is expected to be released by the softening and/or decomposition of the matrix components of the G-layer and
566 the lignified secondary walls of the G-fibers by the HT-treatment. During this process, the G-fiber contracts again,

the magnitude of which depends on the HT-treatment temperature since degree of HT-softening of the matrix components is temperature dependent. From the macroscopic point of view, we can consider that the longitudinal HTR-strain can be described as a delayed recovery of viscoelastically-locked tensile growth stress in the G-layer, which is accelerated by HT-softening of the cell wall.

A hypothetical mechanism of origin of drying shrinkage in TW

In the present study, drying shrinkage strain was not measured, even though many results had been ever reported concerning about it by early authors (*e.g.*, Yamamoto et al. 1992; ibid. 2005; ibid. 2010; Abe and Yamamoto 2007; Sujan et al. 2018; Clair and Thibout 2001; Clair et al. 2003; Vilkovska et al. 2019). It is natural to consider that moisture desorption causes a large scale of volumetric shrinkage of matrix component in the G-layer and the lignified layer. This enables the cellulose single crystallites that had been stretched to be recovered. In other words, during the drying process, the G-fiber can contract due to the concerted effect of the remaining tensile stress in the CMF and the drying shrinkage of the matrix component in the G-layer and the lignified layer.

Generation mechanism of maturation strain as a missing link

If the above arguments are correct, we first need to explain why the CMF generates tensile stress when it is formed. Experiment 1 showed that the maximum longitudinal HTR-strain of the TW specimen was about -3[%] when subjected to repeated high temperature treatments of 120[°C]. This indicates that the cellulose crystallite in the G-layer of TW were subjected to tensile stress corresponding to a lattice strain of about 3 [%] or more. Although this does not exceed the proportional limit of the stress-strain curve of a cellulose crystallite (*e.g.*, Wu *et al*. 2014), it is still an unreasonably large value for the lattice strain of cellulose crystallite in vivo. These may suggest that the observed HTR-strain does not originate from the unit cell of cellulose crystallite, but from the structural property of the CMF as an aggregate of several single crystallites. This could be attributed to the twisted structure of the rod-shaped single crystallites of cellulose (e.g., Fernandes et al. 2011; Paavilainen et al. 2011; Conley et al. 2017; Willhammar et al. 2021). According to those authors, it is considered that a single crystallite of cellulose exhibits energy stability by adopting a twisted structure.

In the process of formation of the G-layer, the newly synthesized crystallites of cellulose form the CMF through interaction with the surrounding matrix components and water molecules (*e.g.*, Joseleau et al. 2001; Kim et al. 2002; Fang and Catchmark 2014). At this time, the single cellulose crystallite with the twisted structure will probably be stretched beyond its original length to form the CMF in G-layer. After that, as the deposition of the matrix component is completed, the stretching deformation of the single crystallite is fixed, which causes tensile stress generation in the longitudinal direction in the G-layer. Of course, this is more than a mere speculation with little evidence to support it.

As described in Introduction, several researchers have hypothesized the roles of amorphous globular polysaccharides such as RG-1, AGP, and acidic galactan form in the gaps between CMFs in the G-layer in generating a longitudinal tensile stress in the CMFs of the G-layer (Bowling et al. 2008; Sandquist et al. 2010;

Mellerowicz et al. 2012; Gorshkova et al. 2015; Guede et al. 2017; Almeras and Clair 2016). If so, it would mean that even though amorphous polysaccharides are generally unstable to HT-treatment at temperatures higher than 100 [°C] (Tejada et al., 1998), those globular polysaccharides are thermally stable to high HT-treatment temperatures, unlike the other matrix components of the cell wall. Again, this is not beyond one of the possible ideas and there is still little evidence to support it.

Macroscopic description of time-dependent evolution of longitudinal HTR-strain in TW

Formulation

As mentioned above, from a macroscopic point of view, longitudinal HTR-strain in the G-fiber can be described as the delayed recovery of tensile stress viscoelastically-locked in the G-layer. Based on this idea, Sujan et al. (2016) and Capron et al. (2018) attempted to formulate the time-dependent evolution of the observed HTR-strain. For the simulation, they employed a mathematical model that combines two Voigt-elements in series. As the result, they succeeded in simulating the "initial recovery" and "continuum contraction" which are observed specifically in the G-fiber. In this subchapter, their simulation will be further generalized to quantitatively explain evolutions of the longitudinal HTR-strains revealed in Experiment 1. Detailed process of formulation was described in Appendix of this paper.

Assume that the TW specimen was subjected to HT-treatment at temperature θ_1 ($> \theta_0$), where θ_0 is the threshold temperature. The longitudinal HTR-strain $\varepsilon_L(t, \theta_1)$ in the G-fiber is formulated by the following equation (see Appendix A)

$$\varepsilon_L(t,\theta_1) = \int_{\theta_0}^{\theta_1} (1 - e^{-k(\theta,\theta_1)t}) a_L^0 \, d\theta \tag{6}$$

where a positive value $k(\theta, \theta_1)$ is a two-variable function of θ (satisfies $\theta_0 < \theta < \theta_1$) and the treatment temperature θ_1; this corresponds to the retardation time of the Voigt-element. Hereafter, we refer parameter θ as “hidden temperature of the treatment temperature θ_1”. In other words, $k(\theta, \theta_1)$ represents the degree of ease of softening of cell wall component that becomes soften at temperature θ under the HT-treatment temperature θ_1. The constant a_L^0 is the gradient of the linear equation (5), that is, $a_L^0 = -0.0339$ [%/°C].

From the microscopic point of view, cell wall softening would occur in the matrix components as discussed above. It is considered that the matrix component of the G-layer consists of many kinds of amorphous polysaccharides, each of which has its own softening temperature θ ($\theta_0 < \theta < \theta_1$) and the softening rate of each is affected also by the treatment temperature θ_1, which would be formulated as the function $k(\theta, \theta_1)$. From eq.(6), we can see that evolution of the longitudinal HTR-strain $\varepsilon_L = \varepsilon_L(t, \theta_1)$ is determined by the functional form of $k(\theta, \theta_1)$, which is calculated back through reproducing the observed longitudinal HTR-strain by using Eq.(6). It is sufficient to discuss the physical meaning of the θ-dependence of back-calculated function $k(\theta, \theta_1)$.

Assumptions for simulations

Equation (6) was used to simulate the time-dependent evolution of $\varepsilon_L = \varepsilon_L(t, \theta_1)$ for the cases θ_1= 60, 80, 100, and 120 [°C]. Results of simulation were compared with the observations in Phase 1 of Experiment 1. In this simulation, we assume that $k(\theta, \theta_1)$ varies continuously in the temperature range of $\theta_0 < \theta < \theta_1$. The following cases are tested for the function $k(\theta, \theta_1)$.

Case 1: $k(\theta, \theta_1)$ is independent of θ, but depends on the treatment temperature θ_1, and $k(\theta, \theta_1)$ increases with θ_1. In other words, we assume that the degree of HT-softening is uniform regardless of the hidden temperature θ, and softening rate increases with θ_1.

Case 2: $k(\theta, \theta_1)$ becomes larger as the absolute value of the difference between θ_1 and θ becomes larger. This means that the softening of the matrix components at a certain hidden temperature θ proceeds faster as the difference between the HT-treatment temperature θ_1 and θ becomes larger.

Figures 11 and **12** show results of the simulations based on the above assumptions.

Result of simulation

Eq.(6) explains that the evolution of the longitudinal HTR-strain of the G-fiber depends on the HT-treatment temperature. For the pattern of evolution of longitudinal HTR-strain, *Case 1* can only explain either the occurrence of "continuous contraction" or the occurrence of "initial recovery". That is, the former is explained by relatively smaller $k(\theta, \theta_1)$ (**Fig. 11(a)**), while the latter is explained by larger $k(\theta, \theta_1)$ (**Fig.11 (b)**). On the other hand, *Case 2* can explain both observed occurrence of "initial recovery" and "continuous contraction" at the same time (see, **Fig. 12**). The result suggests that the softening of the matrix components at a certain hidden temperature θ proceeds more rapidly as the difference between the treatment temperature θ_1 and θ becomes larger.

Fig. 11 Simulated results of evolutions of longitudinal HTR-strains in the treatment of Phase 1 of Experiment 1 (upper panels). Lower panels show assumptions of θ-dependencies of function $k(\theta, \theta_1)$ (θ_1 = 60, 80, 100, and 120 [°C]). *Case 1* was adopted: $k(\theta, \theta_1)$ is independent of θ and depends on the treatment temperature θ_1. Furthermore, the simulation was performed assuming that $k(\theta, \theta_1)$ increases with θ_1. (a): A subcase for comparatively smaller $k(\theta, \theta_1)$ (b) A subcase for comparatively larger $k(\theta, \theta_1)$.

In both simulations, when the treatment temperature is 120 [°C] and the treatment time exceeds 1000 [min], there is a slight deviation between the observed and simulated values. The former is larger than the latter in absolute value. This is because Eq. (6) does not take into account shrinkage due to decomposition and lelution of matrix components at treatment temperatures above 115 [°C]. In general, it can be said that *Case 2* gives more reasonable results, but it is only one of the possible sufficient conditions to explain the observed time-dependent evolution of the longitudinal HTR-strain, and so far it is not beyond the realm of hypothesis.

Fig. 12 Simulated results of evolutions of longitudinal HTR-strains in the treatment of Phase 1 of Experiment 1 (upper panels). Lower panels show assumptions of θ-dependencies of function

680 $k(\theta, \theta_1)$ (θ_1 = 60, 80, 100, and 120 [°C]). *Case 2* was adopted: $k(\theta, \theta_1)$ becomes larger with the
681 absolute difference between θ_1 and θ. This assumes that the softening of the matrix components
682 at a certain hidden temperature θ proceeds faster as the difference between θ_1 and θ becomes
683 larger.
684
685 # Conclusion
686
687 This study aimed to explain why tension wood (TW), which is composed of gelatinous fibers (G-fiber), contracts in
688 the longitudinal direction upon HT-treatment. For this purpose, developed TW specimens of Konara oak (*Quercus*
689 *serrata*) were subjected to the HT-treatment at temperatures of 40, 50, 60, 70, 80, 90, 100, 115, and 120 [°C], and
690 hygrothermal recovery strain (HTR-strain) in TW specimen was followed during the HT-treatment (Experiment 1).
691 The mass loss due to HT-treatment at treatment temperatures of 80, 100, and 120 [°C] was also followed to
692 compare with the time-dependent evolution of the HTR-strain (Experiment 2). Obtained results are summarized as
693 follows.
694 *Experiment 1:*
695 (R1) Green TW specimen of Konara oak contracted in the longitudinal direction when subjected to the HT-
696 treatment at a treatment temperature higher than 40 [°C], which eventually converged to a constant value
697 according to each treatment temperature. Magnitude of the longitudinal HTR-strain in a typical TW was
698 positively correlated with the treatment temperature.
699 (R2) Green NW specimen showed almost no longitudinal contraction nor elongation at a treatment temperature
700 bellow 100 [°C]; however, it contracted linearly and continuously as the treatment proceeds when subjected to
701 the HT-treatment at a treatment temperature higher than 115 [°C].
702 *Experiment 2:*
703 (R3) Both TW and NW specimens showed mass loss when subjected to the HT-treatment. The mass loss rate
704 increased rapidly at 120[°C] treatment, while it was only slight at the HT-treatment below 100[°C]. The
705 progressive mass loss at 120[°C] in Experiment 2 was consistent with a rapid decrease in the tangential HTR-
706 strain in the TW and NW specimen and the linear increase in the negative value of longitudinal HTR-strain in
707 the NW specimen in Experiment 1. There was no significant difference between the mass loss behavior of TW
708 and NW by the HT-treatment.
709
710 From the obtained results, the following conclusions were made:
711 (C1) A tensile stress is generated in the CMF in the G-layer during its maturation. This induces the longitudinal
712 tensile growth stress in the G-fiber of living TW.
713 (C2) Some of the tensile stress in the CMF is elastically released by separating the wood specimen from the living
714 stem, but much of the tensile stress still remains in the G-layer without being released. This stress is released
715 by the softening and/or decomposition of the matrix component by HT-treatment. In this process, TW shows a
716 longitudinal contraction, that is, the longitudinal-HTR-strain.
717 (C3) Moisture desorption causes a large scale of volumetric shrinkage of matrix component in the G-layer. This
718 enables the CMF that had been stretched to be recovered. In other words, the drying process allows the G-fiber

to longitudinally contract due to the concerted effect of the remaining tensile stress in the CMF and the shrinking stress of the matrix substance in the G-layer.

(C4) From a macroscopic point of view, the longitudinal HTR-strain can be formulated as a delayed recovery of tensile growth stress viscoelastically-locked in the G-layer, which is accelerated by HT-treatment at temperatures higher than the threshold temperature.

Acknowledgements We thank Mr. Naoki Takabe and Mr. Norio Yamaguchi of the Nagoya University Experimental Forest (Inabu-cho, Toyota-City, Aichi-Prefecture, Japan) for their technical cooperation in selecting and sampling the material trees. We would also like to thank the Isotope Research Center of Nagoya University (Chikusa-ku, Nagoya, Japan) for their cooperation in the XRD measurements.

Funding This work was financially supported by the Graduate Program of Transformative Chem-Bio Research (GTR), Nagoya University (Chikusa-ku, Nagoya, Japan).

Declarations

Conflict of Interest The authors declare that they have no conflict of interest.

References

Abe K, Yamamoto H (2007) The influence of boiling and drying treatments on the behaviors of tension wood with gelatinous layers in *Zelkova serrata*. Journal of Wood Science 53:5-10.

Agarwal UP, Ralph SA, Baez C, Reiner RS, Verrill SP (2017) Effect of sample moisture content on XRD-estimated cellulose crystallinity index and crystallite size. Cellulose 24:1971–1984.

Alméras T, Clair B (2016) Critical review on the mechanisms of maturation stress generation in trees. Journal of Royal Society Interface 13:Article number 20160550.

Araki N, Fujita M, Saiki H, Harada H (1982) Transition of the fiber wall structure from normal wood to tension wood in *Robinia pseudoacacia* L. and *Populus euramericana* Guinier. Mokuzai Gakkaishi 28:267-273.

Baba K, Parka YW, Kaku T, Kaida R, Takeuchi M, Yoshida M, Hosoo Y, Ojio Y, Okuyama T, Taniguchi T, Ohmiya Y, T Kondo, Shani Z, Shoseyov O, Awano T, Serada S, Norioka N, Norioka S, Hayashia T (2009) Xyloglucan for generating tensile stress to bend tree stem. Molecular Plant 2:893–903.

Bowling AJ, Vaughn KC (2008) Immunocytochemical characterization of tension wood: gelatinous fibers contain more than just cellulose. American Journal of Botany 95:655–663

Capron M, Bardet S, Sujan KC, Matsuo UM, Yamamoto H (2.018) Viscoelastic modelling of wood in the process of formation to clarify the hygrothermal recovery behavior of tension wood. Journal of Material Science 53:1487–1496.

Cave ID (1966) Theory of X-ray measurement of microfibril angle. Forest Products Journal 16:37-42.

Chen S, Matsuo-Ueda M, Yoshida M, Yamamoto H (2021) Hygrothermal recovery behavior of cellulose-rich gelatinous layer in tension wood studied by viscoelastic vibration measurement. Cellulose 28:5793–5805.

Clair B (2012) Evidence that release of internal stress contributes to drying strains of wood. Holzforschung 66:349–353.

Clair B, Thibaut B (2001) Shrinkage of the gelatinous layer of poplar and beech tension wood. IAWA Journal 22:121-131.

Clair B, Ruelle J, Thibaut B (2003) Relationship between growth stress, mechanical-physical properties and proportion of fibre with gelatinous layer in chestnut (*Castanea Sativa* Mill.). Holzforshung 57:189-195.

Clair B, Gril J, Di Renzo F, Yamamoto H, Quignard F (2008) Characterization of a gel in the cell wall to elucidate the paradoxical shrinkage of tension wood. Biomacromolecules 9:494-498.

Conley K, Whitehead MA, van de Ven TGM (2017) Probing the structural chirality of crystalline cellulose with induced circular dichroism. Cellulose 24:479–486.

Côté WA Jr, Day AC (1962) The G-layer in gelatinous fibers - electron microscopic studies. Forest Products Journal 17:333–339.

Fang L, Catchmark JM (2014) Structure characterization of native cellulose during dehydration and rehydration. Cellulose 21:3951–3963.

Fengel D, Wegener G (1984) Wood - chemistry, ultrastructure, and reactions. De Gruyter, Berlin, New York.

Fernandes AN, Thomas LH, Altaner CM, Callowd P, Forsythd VT, Apperley DC, Kennedy CJ, Jarvish MC (2011) Nanostructure of cellulose microfibrils in spruce wood. PNAS 108:E1195–E1203.

Fourcaud T, Lac P (2003) Numerical modelling of shape regulation and growth stresses in trees I. An incremental static finite element formulation. Trees 17:23–30.

Garrote G, Dominguez H, Parajo JC (2001) Study on the deacetylation of hemicelluloses during the hydrothermal processing of Eucalyptus wood. Holz als Roh- und Werkstoff 59:53-59.

Goring DAI (1963) Thermal softening of lignin, hemicellulose and cellulose. Pulp Paper Magazine of Canada 64:T517-527.

Gorshkova T, Mokshina N, Chernova T, Ibragimova N, Salnikov V, Mikshina P, Tryfona T, Banasiak A, Immerzeel P, Dupree P, Mellerowicz EJ (2015) Aspen tension wood fibers contain beta-(1--->4)- galactans and acidic arabinogalactans retained by cellulose microfibrils in gelatinous walls. Plant Physiology 169: 2048-2063.

Gril J, Berrada E, Thibaut, B (1993) Recouvrance hygrothermique du bois vert II. Variations dans le plan transverse chez le Châtaignier et l'Epicéa et modélisation de la fissuration à coeur induite par l'étuvage. Annales des Sciences Forestières 50:487-508 (in French with English summary).

Gril J, Thibaut B (1994) Tree mechanics and wood mechanics. Relating hygrothermal recovery of green wood to the maturation process. Annales des Sciences Forestières 51:329-338.

Gril J, Bardet S, Julien D, Yamamoto H (2017) Tree growth stress and its problems. Journal of Wood Science 63:411-432.

Guedes FTP, Laurans F, Quemener B, Asso C, Lainé-Prade V, Boizot N, Vigouroux J, Lesage-Descauses MC, Jean-Charles Leplé JC, Déjardin A, Pilate G (2017) Non-cellulosic polysaccharide distribution during G-layer formation in poplar tension wood fibers: abundance of rhamnogalacturonan I and arabinogalactan proteins but no evidence of xyloglucan. Planta 246:857–878.

Joseleau JP, Imai T, Kuroda K, Ruel K (2004) Detection in situ and characterization of lignin in the G-layer of tension wood fibres of Populus deltoides. Planta 219:338–345.

Kang KY, Bradic S, Avramidis S, Mansfield SD (2007) Kiln-drying lumber quality of hybrid poplar clones. Holzforschung 61:65–73.

Kim YS, Wi SG, Grunwald C, Schmitt U (2002) Immuno electron microscopic localization of peroxidases in the differentiating xylem of *Populus* spp. Holzforschung 56:355–359.

794 Kim DY, Nishiyama Y, Wada M, Kuga S, Okano T (2001) Thermal decomposition of cellulose crystallites in wood. Holzforschung
795 55:521-524.
796 Kübler H (1959) Studien über wachstumsspannungen des holzes III. Längenänderungen bei der wärmebehandlung frischen holzes (in
797 German). Holz als Roh- und Werkstoff 17:77-86.
798 Kübler H (1988) Growth stresses and related wood properties. Forest Product Abstracts 10:61-119.
799 Kübler H, Chen T (1974) How to cut tree disks without formation of checks. Forest Products Journal 24:57-59.
800 Leppanen K, Bjurhager I, Peura M, Kallonen A, Suuronen JP, Penttila P, Love J, Fagerstedt K, Serimaa R (2011) X-ray scattering and
801 microtomography study on the structural changes of never-dried silver birch, European aspen and hybrid aspen during drying.
802 Holzforschung 65:865–873.
803 Matsuo MU, Niimi1 G, Sujan KC, Yoshida M, Yamamoto H (2016) Hygrothermal recovery of compression wood in relation to elastic
804 growth stress and its physicochemical characteristics. Journal of Material Science. 51:7956-7965.
805 Matsuo-Ueda M, Yoshida M, Yamamoto H (2018) Irreversible dimensional changes of tension wood by boiling - time and
806 temperature dependency (in Japanese). Abstract of the 68th Annual Meeting of The Japan Wood Research Societry in Kyoto, on
807 March 14-16, 2018.
808 Mellerowicz EJ, Immerzeer P, Hayashi T (2008) Xyloglucan: The molecular muscle of trees. Annals of Botany 102:659-665.
809 Mellerowicz EJ, Gorshkova TA (2012) Tensional stress generation in gelatinous fibres: a review and possible mechanism based on
810 cell wall structure and composition. Journal of Experimental Botany 63: 551- 565.
811 Meylan BA (1967) Measurement of microfibril angle by X-ray diffraction. Forest Products Journal 17:51–58.
812 Müller M, Burghammer M, Sugiyama J (2006) Direct investigation of the structural properties of tension wood cellulose microfibrils
813 using microbeam X-ray fibre diffraction. Holzforschung 60:474–479.
814 Nishikubo N, Awano T, Banasiak A, Bourquin V, Ibatullin F, Funada R, Brumer H, Teeri TT, Hayashi T, Sundberg B, Mellerowicz EJ
815 (2007) Xyloglucan endo-transglycosylase (XET) functions in gelatinous layers of tension wood fibers in poplar—A glimpse into
816 the mechanism of the balancing cct of trees. Plant and Cell Physiology 48:843–855.
817 Okuyama T, Sasaki Y, Kikata Y, Kawai N (1981) The seasonal change in growth stress in the tree trunk. Mokuzai Gakkaishi 27: 351-
818 355.
819 Okuyama T, Yamamoto H, Iguchi M, Yoshida M (1990) Generation process of growth stresses in cell walls. II. Growth stress in
820 tension wood. Mokuzai Gakkaishi 36:797-803.
821 Okuyama T, Yamamoto H, Yoshida M, Hattori Y, Archer RR (1994) Growth stresses in tension wood. Role of microfibrils and
822 lignification. Annales des Sciences Forestieres 51:291-300.
823 Okuyama T, Doldan J, Yamamoto H, Ona T (2004) Heart splitting at crosscutting of Eucalyptus grandis logs. Journal of Wood Science
824 50:1-6.
825 Onaka F (1949) Studies on compression and tension wood (in Japanese). Wood Research 1:1-88.
826 Paavilainen S, Tomasz R, Vattulainen I (2011) Analysis of Twisting of Cellulose Nanofibrils in Atomistic Molecular Dynamics
827 Simulations. The Journal of physical chemistry 115:3747–3755.
828 Sandquist D, Filonova L, von Schantz L, Ohlin M, Daniel J (2010) Microdistribution of xyloglucan in differentiating poplar cells.
829 BioResources 5:796-807.
830 Sasaki Y, Okuyama T (1983) Residual stress and dimensional change on heating green wood. Mokuzai Gakkaishi 29:302-307.

Segal L, Creely JJ, Martin AE, Conrad CM (1959) An empirical method for estimating the degree of crystallinity of native cellulose using the X-ray diffractometer. Text Research Journal 29:786–794.

Sujan KC, Yamamoto H, Matsuo M, Yoshida M, Naito K, Shirai T (2015) Continuum contraction of tension wood fiber induced by repetitive hygrothermal treatment. Wood Science and Technology 49:1157–1169.

Sujan KC, Yamamoto H, Matsuo M, Yoshida M, Naito K, Suzuki Y, Yamashita N, Yamaji FM (2016) Is hygrothermal recovery of tension wood temperature-dependent? Wood Science and Technology 50:759-772.

Sujan KC, Yamamoto H, Matsuo-Ueda M, Yoshida M, Asaka K (2018) Delayed recovery of growth stress in tension wood induced by drying and subsequent wetting treatment. Wood Science and Technology 52:1049–1060.

Tanaka M, Yamamoto H, Kojima M, Yoshida M, Matsuo M, Lahjie AM, Hongo I, Arizono T (2014) The interrelation between microfibril angle (MFA) and hygrothermal recovery in compression wood and normal wood of Sugi and Agathis. Holzforschung 68:823-830.

Tarmian A, Sepeher A, Rahimi S (2009) Drying Stress and Strain in Tension Wood: A Conventional Kiln Schedule to Efficiently Dry Mixed Tension/Normal Wood Boards in Poplar. Drying Technology 27:1033–1040.

Toba K, Yamamoto H, Yoshida M (2013) Crystallization of cellulose microfibrils in wood cell wall by repeated dry-and-wet treatment, using X-ray diffraction technique. Cellulose 20:633–643

Tejada A, Okuyama T, Yamamoto H, Yoshida M, Imai T, Ito T (1998) Studies on the softening point of wood powder as a basis for understanding the release of residual growth stresses in logs. Forest Products Journal 48:84-90.

Toba K, Yamamoto H, Yoshida, M (2013) Crystallization of cellulose microfibrils in wood cell wall by repeated dry-and-wet treatment, using X-ray diffraction technique. Cellulose 20:633–643

Vilkovská T, Klement I, Čunderlík I (2019) Longitudinal contraction of reaction and opposite wood during drying process. Wood Research 64:903-912.

Wada M, Okano T, Sugiyama J, Horii F (1995) Characterization of tension and normally lignified wood cellulose in *Populus maximowiczii*. Cellulose 2:223-233.

Wardrop AB, Dadswell HE (1955) The nature of reaction wood IV: variations in cell wall organization of tension wood fibers. Australian Journal of Botany 3:177–189.

Willhammar T, Daicho K, Johnstone DN, Kobayashi K, Liu Y, Midgley PA, Bergström L, Saito T (2021) Local Crystallinity in Twisted Cellulose Nanofibers. ACS Nano 15:2730−2737.

Wu X. Moon RJ, Martini A (2014) Tensile strength of Iβ crystalline cellulose predicted by molecular dynamics simulation. Cellulose Vol.21:2233–2245.

Yamamoto H, Okuyama T, Iguchi M (1989) Measurement of growth stresses on the surface of a leaning stem (in Japanese, with English summary). Mokuzai Gakkaishi 35:595-601.

Yamamoto H, Okuyama T, Sugiyama K, Yoshida M (1992) Generation process of growth stresses in cell walls. IV. Action of the cellulose microfibril upon the generation of the tensile stresses. Mokuzai Gakkaishi 38:107-113.

Yamamoto H, Okuyama T, Yoshida M (1993a) Generation process of growth stresses in cell walls. V. Model of tensile stress generation in gelatinous fibers. Mokuzai Gakkaishi 39:118-125.

Yamamoto H, Okuyama T, Yoshida M (1993b) Method of determining the mean microfibril angle of wood over wide range by the improved Cave's method. Mokuzai Gakkaishi 39:375-381.

Yamamoto H, Yoshida M, Okuyama T (2002) Growth stress controls negative gravitropism in woody plant stems. Planta 216:280-292.

Yamamoto H, Abe K, Arakawa Y, Okuyama T, Gril J (2005) Role of the gelatinous layer (G-layer) on the origin of the physical properties of the tension wood of *Acer sieboldianum*. Journal of Wood Science 51:222-233.

Yamamoto H, Ruelle J, Arakawa Y, Yoshida M, Clair, B, Gril J (2010) Origin of characteristic properties of gelatinous layer in tension wood from Kunugi Oak (*Quercus acctissima*). Wood Science and Technology 44:149~163.

Yokota T, Tarkow H (1962) Changes in dimension on heating green wood. Forest Products Journal 12:43-45.

Yoshida M, Okuyama T (2002a) Techniques for measuring growth stress on the xylem surface using strain and dial gauges. Holzforschung 56:461-467

Appendix. A macroscopic description of time-dependent evolution of longitudinal HTR-strain in TW specimen (G-fiber)

Assume that the TW specimen (= G-fiber) is subjected to temperature treatment at the actual temperature θ_1 ($> \theta_0$). If the specimen is hypothetically subjected to HT-treatment at a temperature θ lower than the actual treatment temperature θ_1 ($\theta_0 < \theta < \theta_1$), the maximum longitudinal HTR-strain will be given by $a_L(\theta)$ (see Eq.5), where we refer to θ as the "hidden temperature" under the actual treatment temperature θ_1. Next, suppose the treatment temperature is infinitesimally increased by $\Delta\theta$, the maximum longitudinal HTR-strain will be increased by $\Delta a_L(\theta)$.

Based on this $\Delta a_L(\theta)$, we introduce a function $\Delta\varepsilon_L(t, \theta, \theta_1)$ which depends on both time t and the actual HT-treatment temperature θ_1, and converges to $\Delta a_L(\theta)$ after a sufficient time. The function $\Delta\varepsilon_L(t, \theta, \theta_1)$ is monotonically decreasing with t and satisfies the following boundary conditions,

$$\Delta\varepsilon_L(0,\theta,\theta_1) = 0, \quad \lim_{t\to\infty} \Delta\varepsilon_L(t,\theta,\theta_1) = \Delta\alpha_L(\theta,\theta_1) = \Delta\alpha_L(\theta)\,. \tag{A1}$$

Then, we introduce a convergent-type function $\psi(t, \theta, \theta_1)$ which is defined as the following equation,

$$\Delta\varepsilon_L(t,\theta,\theta_1) = \Delta\alpha_L(\theta)\psi(t,\theta,\theta_1) \tag{A2}$$

The function $\psi(t, \theta, \theta_1)$ must satisfy the following boundary conditions.

$$\psi(0,\theta,\theta_1) = 0, \quad \lim_{t\to\infty} \psi(t,\theta,\theta_1) = 1 \tag{A3}$$

The temperature range from the threshold temperature θ_0 [℃] (=33 [℃]) to the HT-treatment temperature θ_1 [℃] is divided into N parts, such as θ_0, θ_1, ... , θ_N (= θ_1). The relationship between $\Delta a_L{}^i$ (=$\Delta a_L(\theta_i)$) and $\Delta\varepsilon_L{}^i$ (=$\Delta\varepsilon_L(t, \theta_i, \theta_1)$) is as expressed in the following equation.

$$\Delta\varepsilon_L^i = \Delta\varepsilon_i(t,\theta_i,\theta_1) = \psi(t,\theta_i,\theta_1)\Delta\alpha_L^i(\theta_i). \tag{A4}$$

It is natural to consider that HT-treatment at temperature θ_1 would superimpose $\Delta\varepsilon_L{}^i$ (i = 0, 1, 2, ..., N) in the temperature range "$\theta_0 < \theta < \theta_1$", resulting in the longitudinal HTR-strain

$$\varepsilon_L(t,\theta_1) = \sum_{i=0}^{N} \Delta\varepsilon_L^i = \sum_{i=0}^{N} \psi(t,\theta_i,\theta_1)\Delta\alpha_L^i = \sum_{i=0}^{N} \psi(t,\theta_i,\theta_1)\Delta\alpha_L\,(\theta_i). \tag{A5}$$

Assuming $N\to\infty$, Eq.(A5) can be rewritten as,

$$\varepsilon_L(t,\theta_1) = \int_{\theta_0}^{\theta_1} \psi(t,\theta,\theta_1)\, da_L(\theta) \;= \int_{\theta_0}^{\theta_1} \psi(t,\theta,\theta_1)\left(\frac{da_L}{d\theta}\right) d\theta\,. \tag{A6}$$

902 Since θ_1 is fixed as the treatment temperature that has been given in advance, the HTR-strain $\varepsilon_L(t, \theta_1)$ is
903 substantially a one-variable function of t; while, it should be noticed the integral (A6) is affected by the θ-
904 dependent function $\psi(t, \theta, \theta_1)$, where θ is a hidden temperature. How does the function $\psi(t, \theta, \theta_1)$ affect the HTR-
905 behaviors of TW will be numerically discussed in the text.
906 In the present study, Experiment 1 and 2 suggested that function $\Delta\varepsilon_L(t, \theta, \theta_1)$ in Eq.(A2) is induced by HT-
907 softening of the matrix component in the cell wall of the G-fiber. It is considered that HT-softening is a simple
908 physical state change in the cell wall components, and thus, it proceeds in a manner of the *first-order reactive* or the
909 *creep-recovery function*. Therefore, it is rather natural to assume the following *first-order reactive* function (i.e.,
910 creep-recovery function) as $\psi(t, \theta, \theta_1)$,

911 $$\psi(t, \theta, \theta_1) = 1 - e^{-k(\theta, \theta_1)t}, \tag{A7}$$

912 where $k(\theta, \theta_1)$ is the constant of reaction rate of *the first-order reaction*, which corresponds to the retardation time
913 of the Voigt-element. The function (A7) satisfies the boundary conditions (A3). Eq.(A6) is rewritten as

914 $$\varepsilon_L(t, \theta_1) = \int_{\theta_0}^{\theta_1} (1 - e^{-k(q;\theta_1)t}) \left(\frac{da_L}{d\theta}\right) d\theta \,. \tag{A8}$$

915 If we accept the result of Eq.(5), that is, $a_L(q) = a_L{}^0(\theta - \theta_0)$, the above integration becomes,

916 $$\varepsilon_L(t, \theta_1) = \int_{\theta_0}^{\theta_1} (1 - e^{-k(\theta, \theta_1)t}) a_L^0 \, d\theta. \tag{A9}$$

917
918

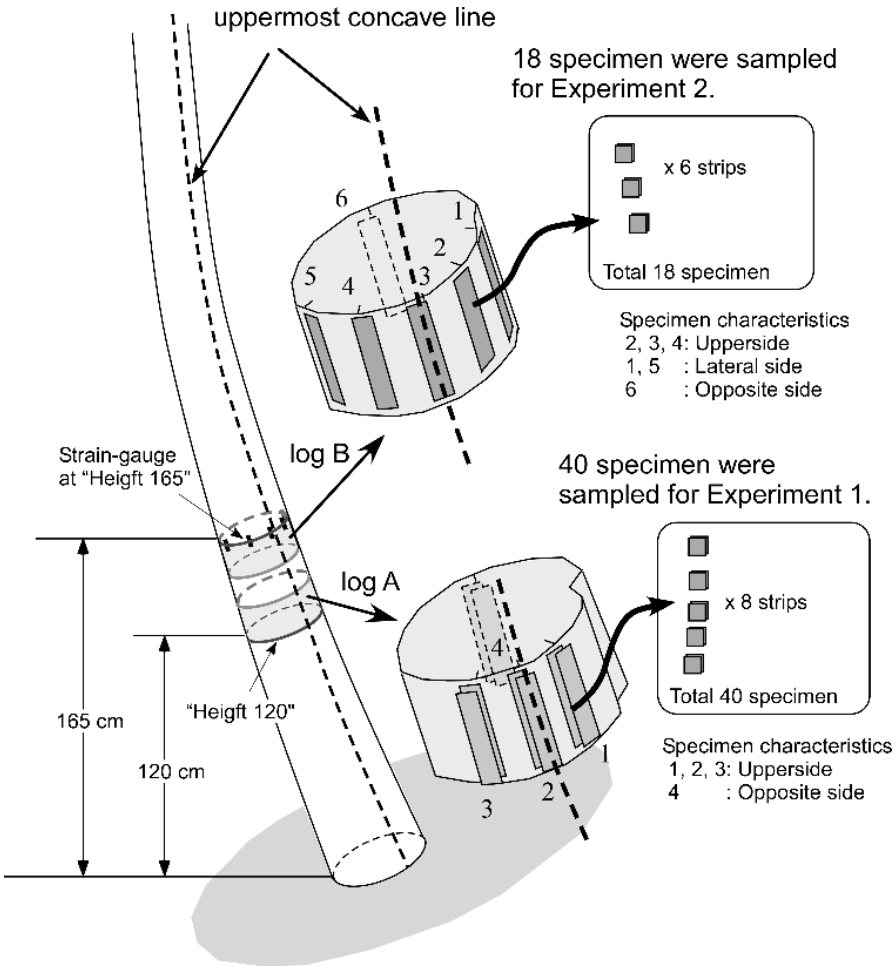

Fig. 1 Schematic representation of tested tree and specimen preparation

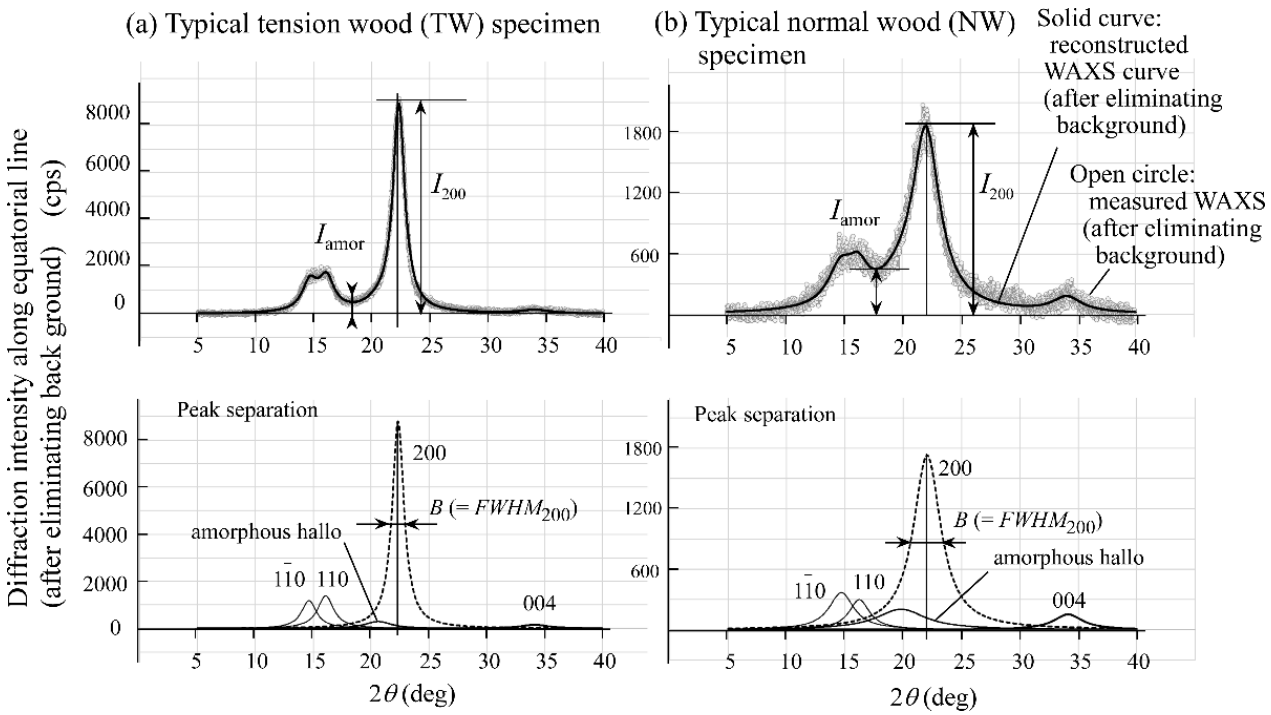

Fig. 2 Typical WAXS profiles of solid wood sections of (a) TW and (b) NW. From WAXS profile, values of *C.I.* (crystallinity index) and *WSC* (width of single crystallites) of CMF are calculated using Eqs.(3) and (4), respectively. Linear background was already eliminated in each profile.

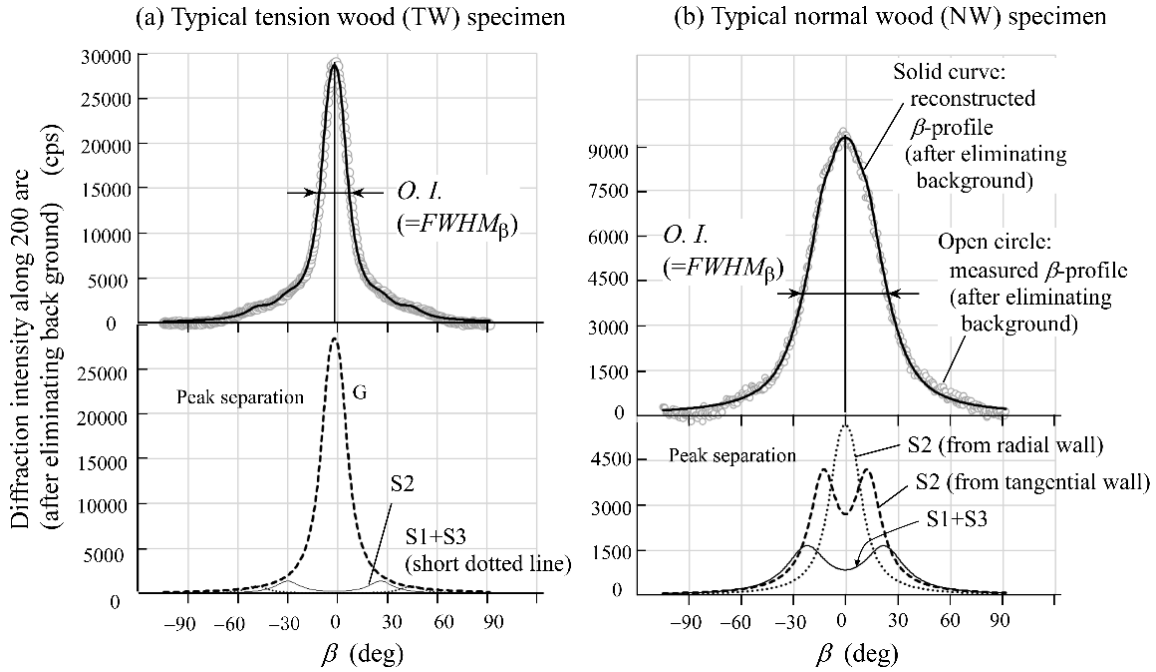

Fig. 3 Typical β-profiles of solid wood sections of (a) TW and (b) NW specimen. From β-profile, an *O.I.*, (= full width of half maximum in the diffraction peak ($FWHM_\beta$)) is calculated. Value of *O.I.* is a convenient indicator of the average MFA in the cell wall. Linear background was already eliminated in each profile.

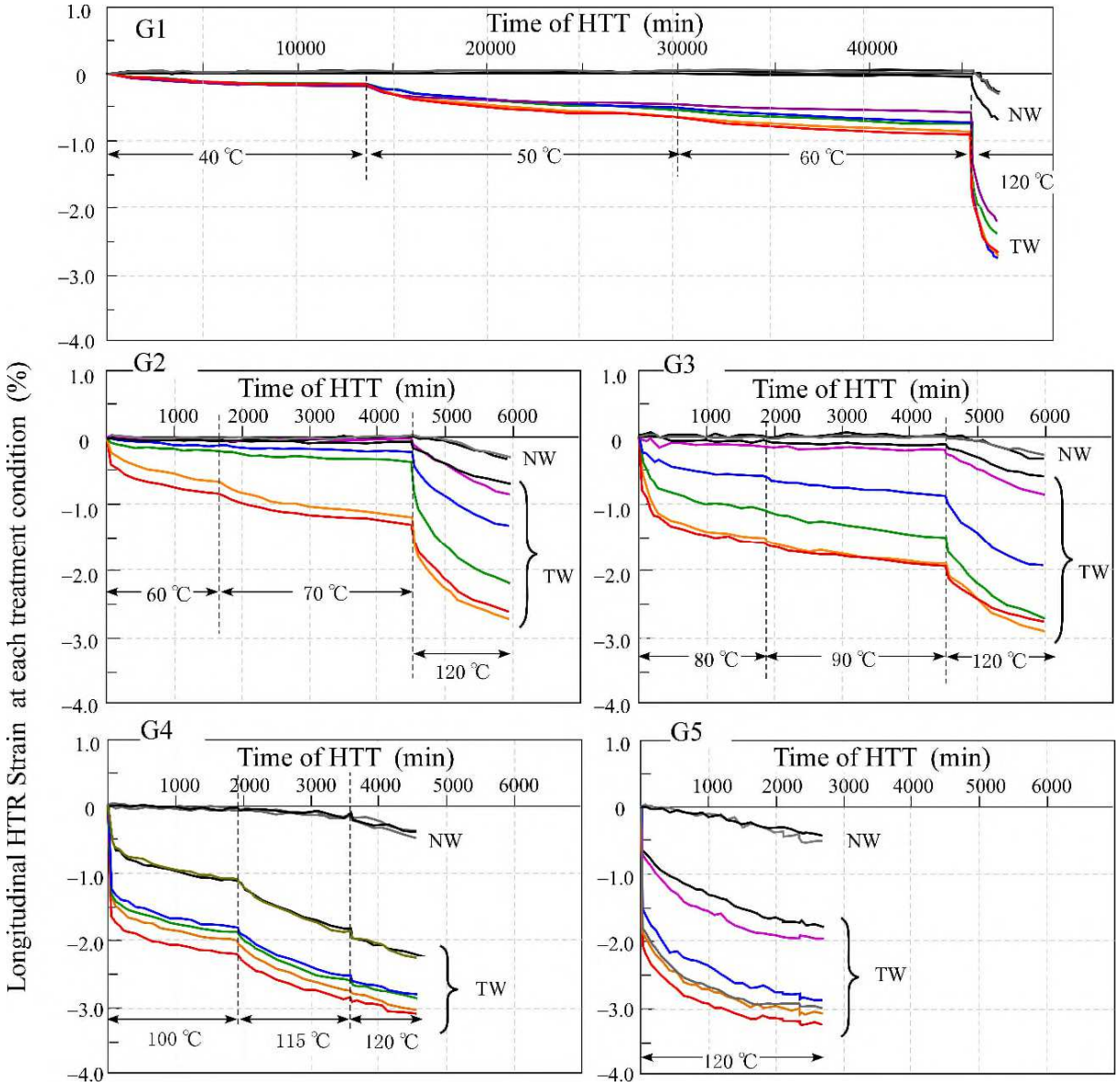

Fig. 4 Time-dependent evolutions of longitudinal HTR-strains in Experiment 1

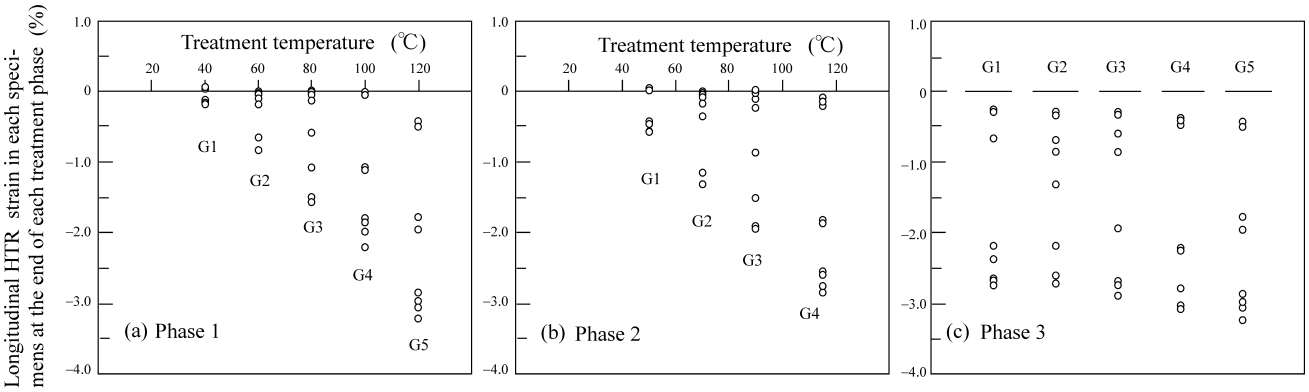

Fig. 5 Longitudinal HTR-strains in each group at the end of Phase 1 (left), Phase 2 (center), and Phase 3 (right)

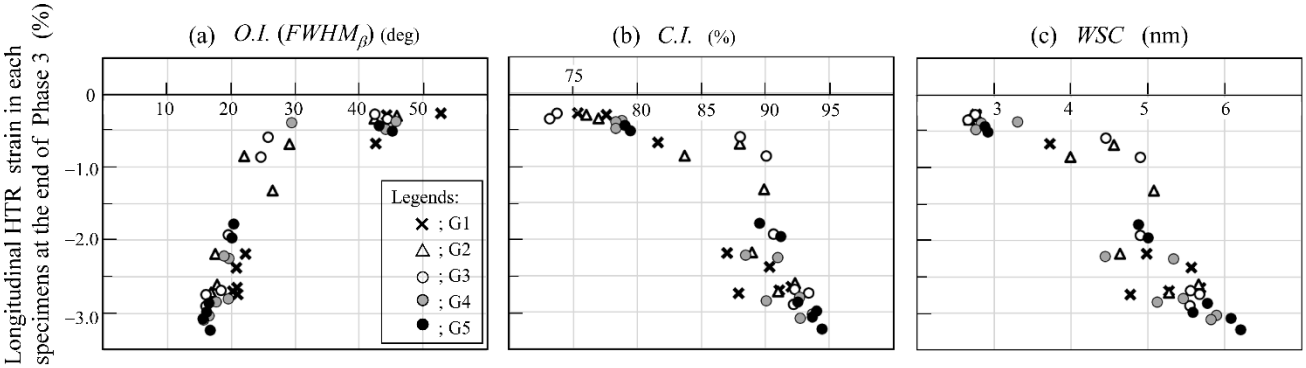

Fig. 6 Correlations of *O.I.* (orientation index, quantified from $FWHM_\beta$ in β-profile), *C.I.* (crystallinity index, calculated by Eq.3), and *WSC* (width of single crystallite of cellulose, calculated by Eq.4) with the longitudinal HTR-strains at the end of Phase 3 in Experiment 1

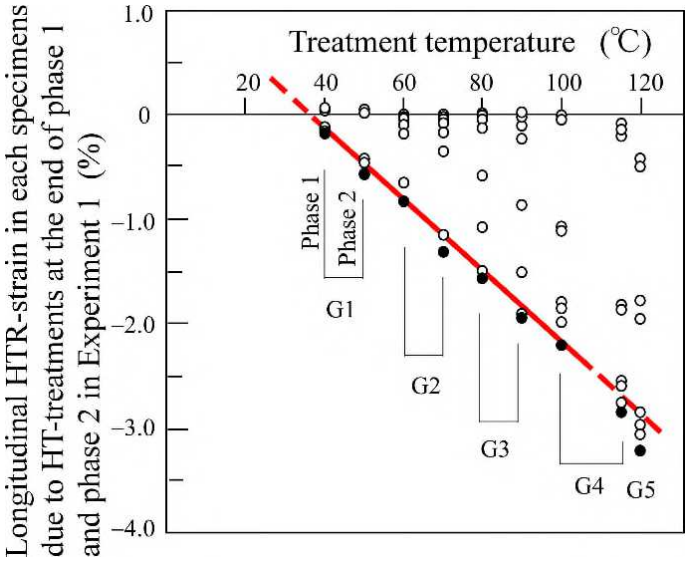

Fig. 7 A composite of Fig. 5a and Fig. 5b. A linear relationship was detected between treatment temperature and the maximum absolute value of longitudinal HTR-strain (solid circle) at the end of Phase 1 and Phase 2 for treatment temperatures below 100 [°C].

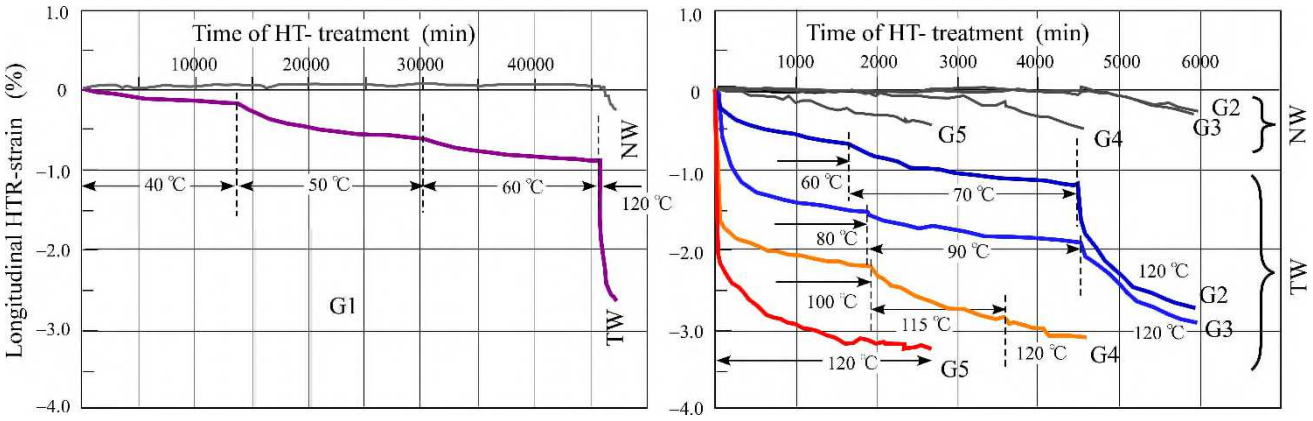

Fig. 8 Time-dependent evolution of longitudinal HTR-strains for TW and NW in Experiment 1. The curves with the largest (highly developed TW) and smallest (NW) absolute values were picked up from each group in Fig. 4, and they were reconstructed as Fig. 8. Values in the figures are treatment temperatures.

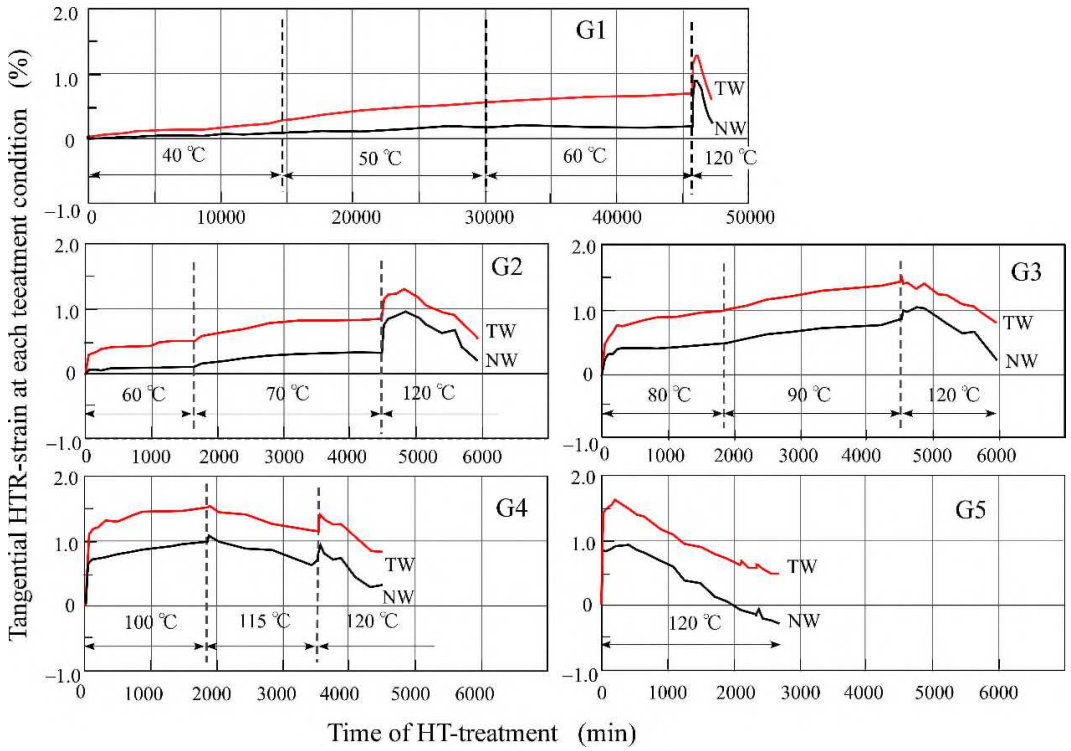

Fig. 9 Time-dependent evolutions of tangential HTR-strains at each treatment group. Displayed curves are for specimens used in Fig. 8.

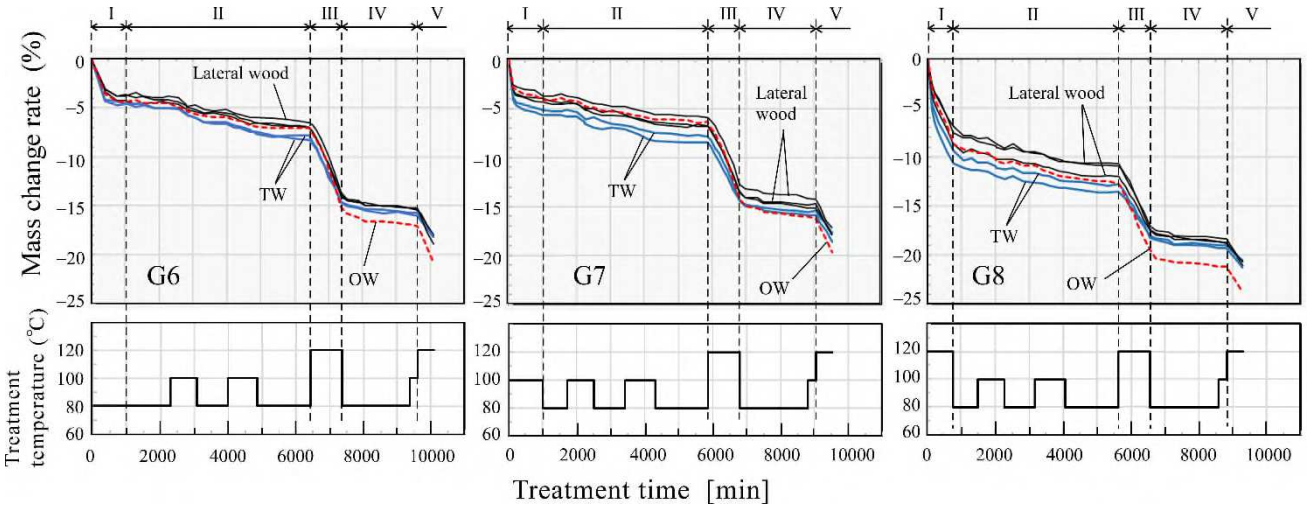

Fig. 10 Mass change rate due to various HT-treatment schedules. Lateral wood specimen often contained G-fiber. Roman numbers on the top of figures stand for HT-treatment phases in Experiment 2.

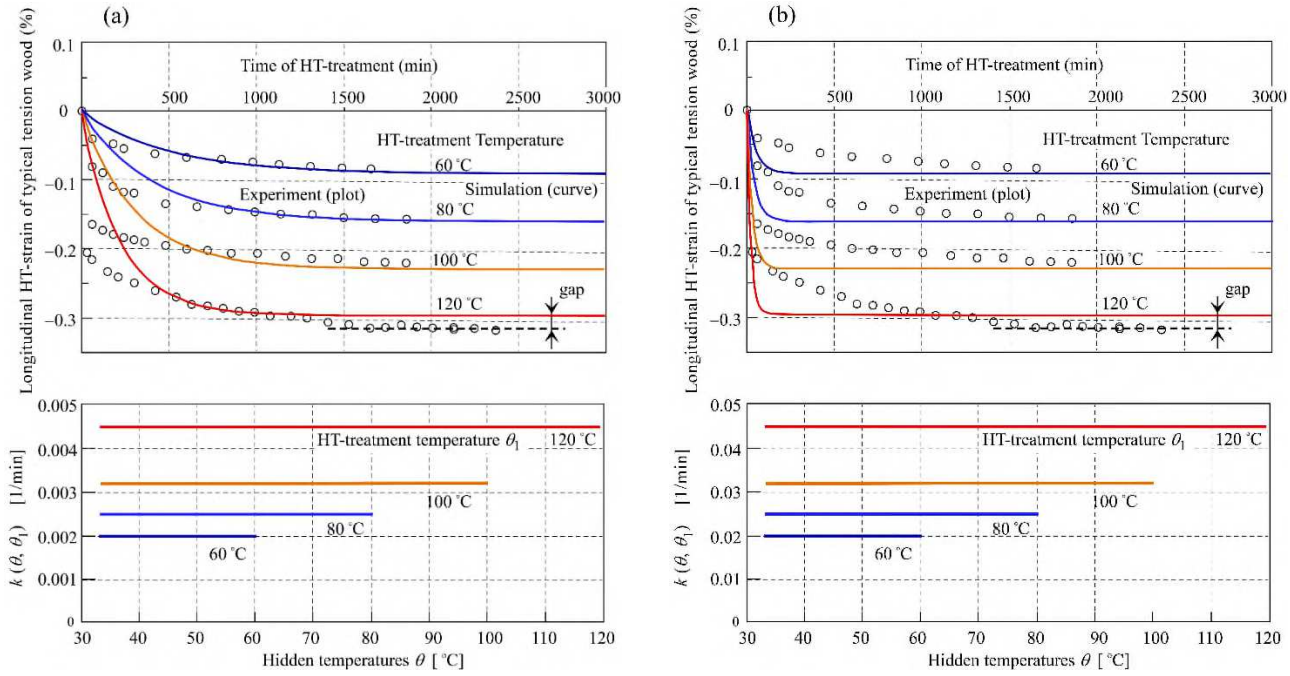

Fig. 11 Simulated results of evolutions of longitudinal HTR-strains in the treatment of Phase 1 of Experiment 1 (upper panels). Lower panels show assumptions of θ-dependencies of function $k(\theta, \theta_1)$ (θ_1 = 60, 80, 100, and 120 [°C]). *Case 1* was adopted: $k(\theta, \theta_1)$ is independent of θ and depends on the treatment temperature θ_1. Furthermore, the simulation was performed assuming that $k(\theta, \theta_1)$ increases with θ_1. (a): A subcase for comparatively smaller $k(\theta, \theta_1)$ (b) A subcase for comparatively larger $k(\theta, \theta_1)$.

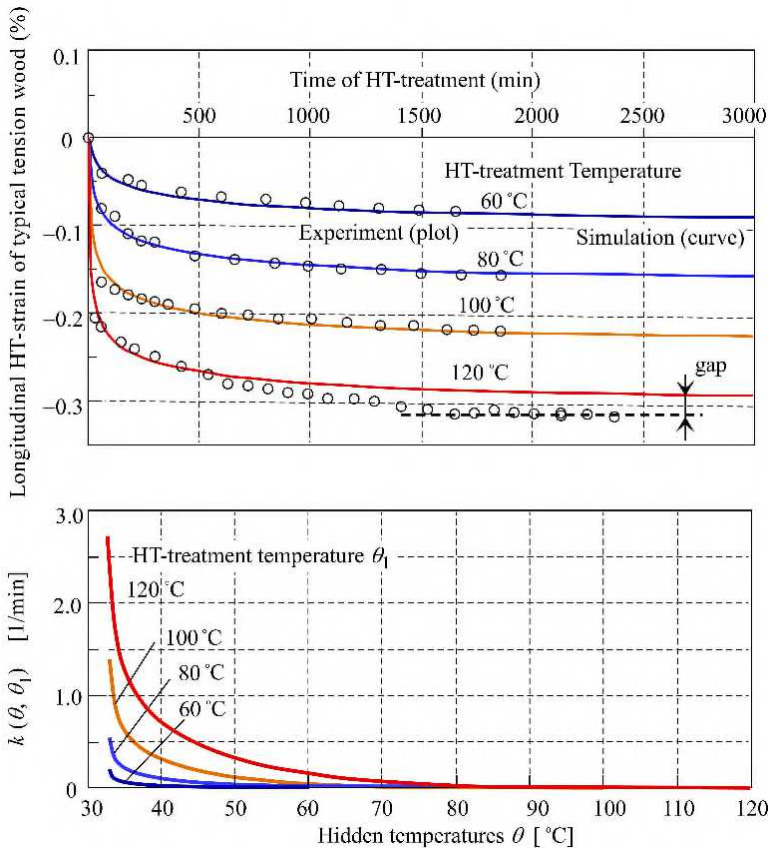

Fig. 12 Simulated results of evolutions of longitudinal HTR-strains in the treatment of Phase 1 of Experiment 1 (upper panels). Lower panels show assumptions of θ-dependencies of function $k(\theta, \theta_1)$ (θ_1 = 60, 80, 100, and 120 [°C]). *Case 2* was adopted: $k(\theta, \theta_1)$ becomes larger with the absolute difference between θ_1 and θ. This assumes that the softening of the matrix components at a certain hidden temperature θ proceeds faster as the difference between θ_1 and θ becomes larger.